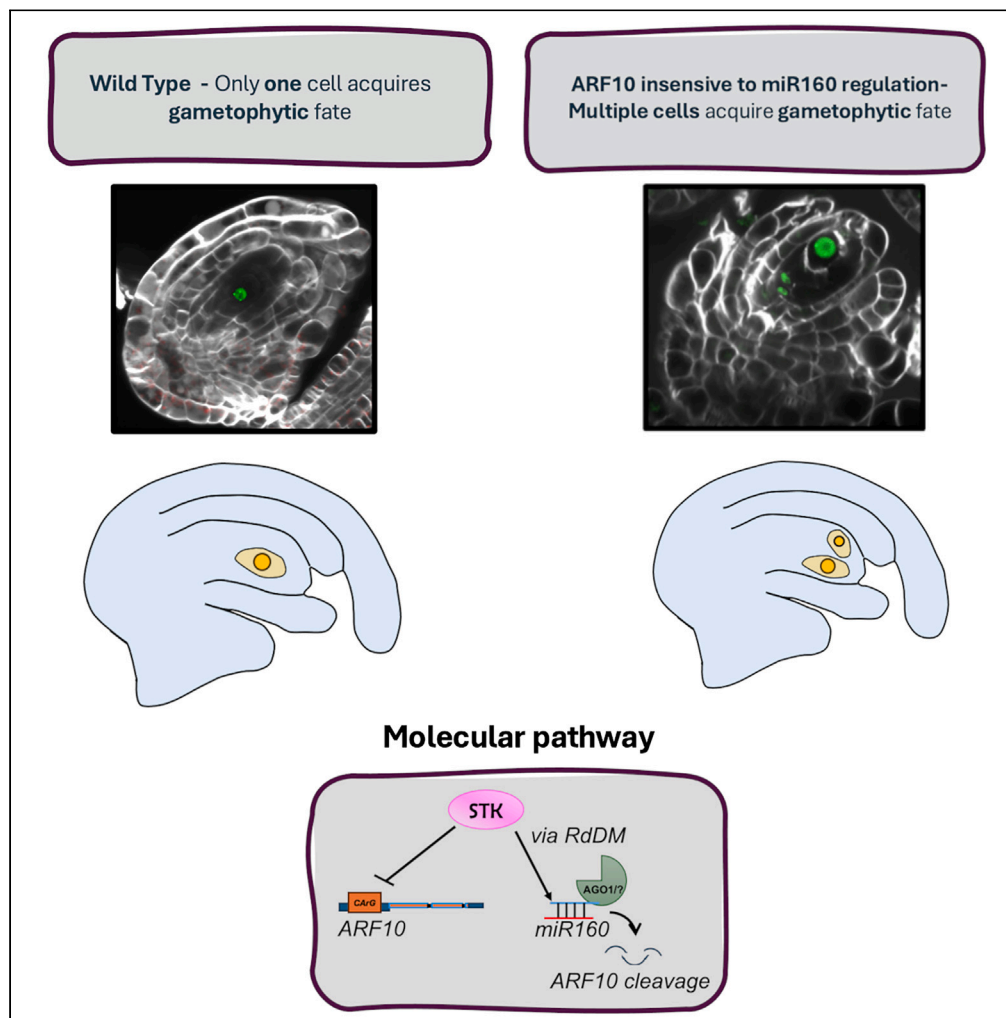


Article

Auxin response factor 10 insensitive to miR160 regulation induces apospory-like phenotypes in *Arabidopsis*



Silvina Pessino, Mara Cucinotta, Carolina Colono, ..., Hugh Dickinson, Lucia Colombo, Marta A. Mendes

marta.mendes@unimi.it

Highlights

Spatial regulation of ARF10 is essential for gametophyte commitment and development

mARF10 lines show multiple functional megaspores and altered gametophytes

ARF10 expression in ovules is controlled by SEEDSTICK, ARGONAUTE1, and miR160

This study could yield tools for advancing plant breeding

Pessino et al., iScience 27, 111115
November 15, 2024 © 2024 The Author(s). Published by Elsevier Inc.
<https://doi.org/10.1016/j.isci.2024.111115>

Article

Auxin response factor 10 insensitive to miR160 regulation induces apospory-like phenotypes in *Arabidopsis*

Silvina Pessino,¹ Mara Cucinotta,² Carolina Colono,¹ Elena Costantini,² Davide Perrone,² Maurizio Di Marzo,² Giada Callizaya Terceros,² Rosanna Petrella,² Chiara Mizzotti,² Celeste Azzaro,¹ Maricel Podio,¹ Gianpiero Marconi,³ Emidio Albertini,³ Hugh Dickinson,⁴ Lucia Colombo,² and Marta A. Mendes^{2,5,*}

SUMMARY

The *Arabidopsis* megaspore mother cell (MMC) arises from somatic cells in the ovule primordium and enters meiosis to generate four megaspores. Only the most chalazal (functional megaspore, FM) survives, undergoing a series of mitoses to form the female gametophyte. We show that this commitment to the sexual germline requires spatial regulation of *AUXIN RESPONSE FACTOR 10* (*ARF10*). GFP-fusion lines reveal *ARF10* expression to be restricted to cells surrounding the MMC in wild type, but ectopically disseminated throughout the ovule in transgenic *mARF10* lines insensitive to miR160, an *ARF10* downregulator. Significantly, *mARF10* ovules develop multiple FMs with differing ploidies, forming putative supernumerary gametophytes with altered polarity and cell identities – features of aposporous apomixis. Furthermore, we confirm the complexity of ovular *ARF10* expression, being mediated by *SEEDSTICK*, *ARGONAUTE1*, and miR160. This work adds to our understanding of molecular switches possibly regulating aposporous apomixis, and may contribute the development of innovative plant breeding strategies.

INTRODUCTION

Flowering plants form seeds using two different mechanisms known as sexual and apomictic reproduction.¹ In the sexual pathway, a meiotic division in the ovule primordia generates a reduced functional megaspore (FM) that, after a regulated series of mitoses, forms a female gametophyte containing two gametes: the haploid egg and the diploid central cell. Double-fertilization of these cells' gametes by two pollen sperm nuclei then leads to production of the embryo and endosperm – key components of the developing seed. By contrast, apomixis (i.e., agamospermy) involves the formation of seeds without previous reductional division, with embryos spontaneously generated through parthenogenesis, and endosperm formed either autonomously, or after pseudogamy (fertilization of the central cell only).² While sexuality leads to genetic variation and syngamy, apomixis generates clonal progeny genetically identical to the mother plant.³ Apomictic mechanisms are usually subcategorized as *sporophytic*, in which nucellar or integumental cells form maternal somatic embryos, or *gametophytic*, in which either the megaspore mother cell (MMC) itself (in the case of diplospory) or integumental/nucellar companion cells (in the case of apospory) differentiate in the ovule as non-reduced FMs, and form non-reduced megagametophytes by mitosis that generate parthenogenetic offspring.³

Apospory, the best characterized apomictic mechanism, has been reported in 110 genera belonging to all seven major clades of angiosperms and in most large orders.⁴ Contrary to adventitious embryony, which is predominant in fabids, malvids, and lamiids, clear phylogenetic tendencies are not apparent for apospory.⁴ It involves the development of extra non-reduced FMs (apospory initials or AIs) from the integuments and/or the nucellus, which are located around the legitimate MMC, the meiotic products and/or the reduced FM. Mature ovules typically feature one or more misoriented non-reduced embryo sacs of variable morphology, which can coexist with the legitimate sexually derived embryo sacs, or alternatively outcompete them.⁵

Female germline development in the model species *Arabidopsis thaliana*, which reproduces exclusively sexually, has been studied intensively in recent years.^{6–9} The process commences with the specification of a single subepidermal cell as the germline precursor, its enlargement to form the MMC, and its entry into meiosis. One of the four meiotic products, the FM, then initiates a controlled series of mitosis to form the mature gametophyte. A multitude of molecular mechanisms is required to establish MMC fate, and to regulate its subsequent

¹Instituto de Investigaciones en Ciencias Agrarias de Rosario (IICAR), Consejo Nacional de Investigaciones Científicas y Técnicas (CONICET), Universidad Nacional de Rosario (UNR), Rosario 2000, Argentina

²Dipartimento di Bioscienze, Università degli Studi di Milano, Via Celoria 26, 20133 Milano, Italy

³Dipartimento di Scienze Agrarie, Alimentari e Ambientali, Università degli Studi di Perugia, 06121 Perugia, Italy

⁴Department of Biology, University of Oxford, South Parks Road, Oxford OX1 3RB, UK

⁵Lead contact

*Correspondence: marta.mendes@unimi.it
<https://doi.org/10.1016/j.isci.2024.111115>



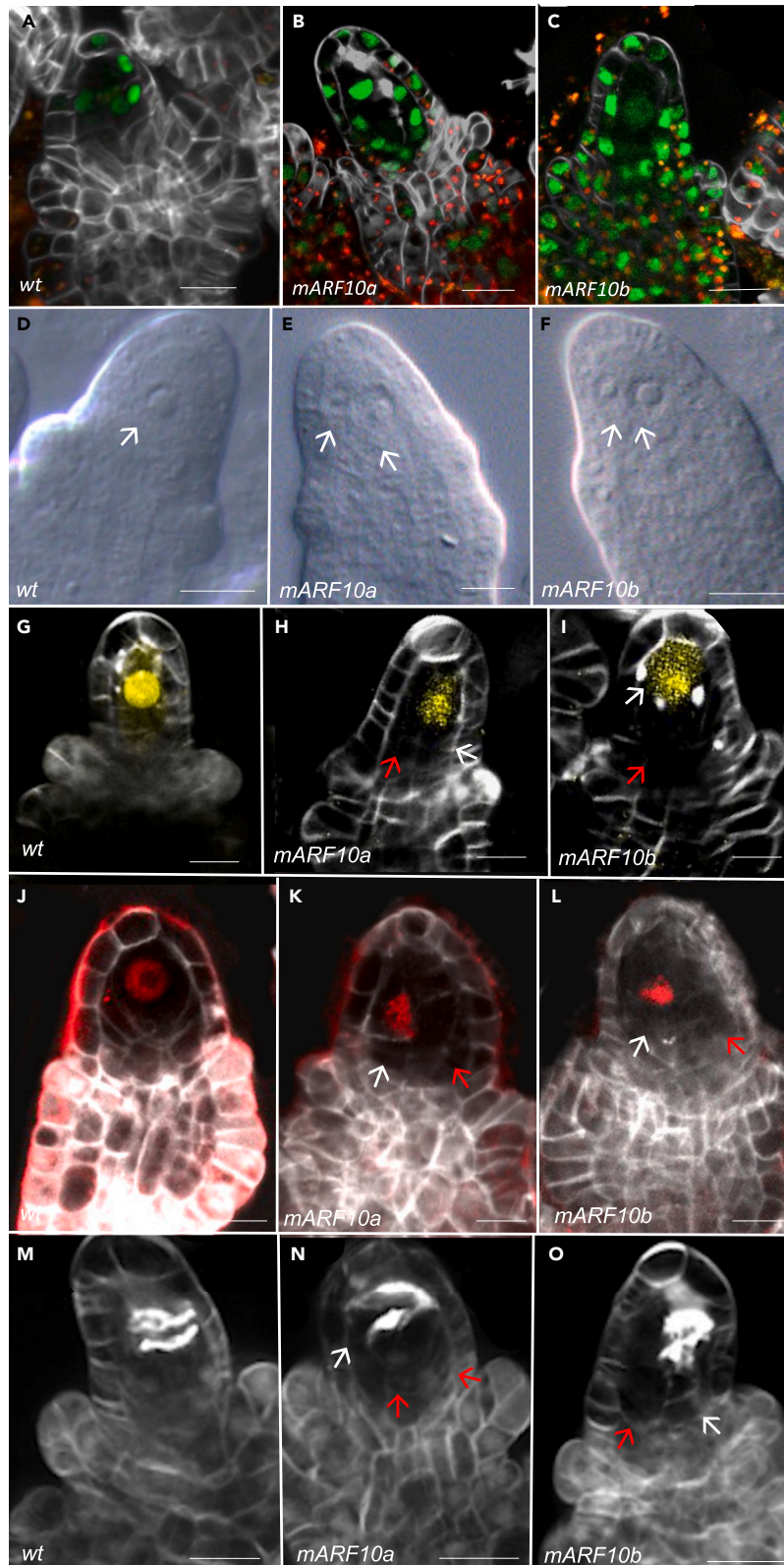


Figure 1. Enlarged cells surrounding the MMC were identified in *mARF10_GFP* lines

(A) *ARF10_GFP* expression at pre-meiosis is detected in a few cells surrounding the MMC (L1 and L2 layers).

(B and C) *mARF10_GFP* expression pattern (lines a and b), at pre-meiosis a strong GFP signal is detected in all ovule cells, including the MMC.

(D) DIC analysis in WT.

(E and F) DIC analysis in *mARF10* lines a and b, respectively; white arrows indicate multiple enlarged cells.

(G) *pKNU:nlsYFP* expression in WT.

(H and I) *pKNU:nlsYFP* expression in *mARF10a* and *b*, respectively; the YFP signal was detected only in one of the enlarged cells (white arrows), often displaced to one side by the presence of extra enlarged cells (red arrows).

(J–L) Meiotic marker *ASY:RFP* in WT and *mARF10* lines. In the transgenic lines only one of the enlarged cells accumulated the meiotic precursor (white arrows), extra enlarged cell didn't express it (red arrows).

(M–O) Renaissance staining in ovule primordia during meiosis; cell plates accumulating callose are detectable. In the WT context two central plates are identifiable; in the transgenic lines they are often displaced (white arrows), red arrows indicate the extra enlarged cells. Renaissance staining was used for the cell walls in all marker line backgrounds. GFP and YFP signals detects expression, RFP detects autofluorescence. Scale bars:10μm.

differentiation. Importantly, canonical female germline commitment is dependent on a range of non-cell-autonomous and epigenetic pathways. For example, RNA-directed DNA methylation (RdDM) – a crucial epigenetic pathway in plants – has been shown to be required for the establishment of a single germline in the *Arabidopsis* pre-meiotic ovule.¹⁰ Significantly, SEEDSTICK (STK), a MADS-box transcription factor that acts as a master regulator of ovule identity, has recently been reported to directly control the transcription of two major RdDM components, AGO9 and RDR6.¹¹

The phytohormone auxin has also been identified as playing a central part in ovule primordia. Polarity setting in the ovule involves localization of PIN auxin transporter proteins in the external cell layer (L1 layer) and an auxin maximum has been detected at the tip of the ovule primordia, directly above the site of MMC differentiation.^{12,13} Specificity of the auxin response is conferred by Auxin Response Factors (ARFs), transcriptional controllers that select target genes for regulation by the hormone. ARFs bind to auxin-response DNA elements (AuxRE) within the promoters of auxin-regulated genes, and either activate or repress transcription depending on a specific protein domain.¹⁴ ARF activity is controlled by IAA repressors and is promoted in the presence of auxin through AUX/IAA degradation. However, it has recently been shown that an ARF5/MP alternative isoform could function as a transcriptional activator within the ovule, even in regions of subthreshold auxin concentration.¹⁵ Some clades of the ARF family are modulated by the THO complex, for example THO/TREX was shown to repress the formation of extra MMCs, mediated by the TAS3-ARF3 module.¹⁶ Other ARFs, such as ARF6/ARF8 and ARF10/ARF16/ARF17, are regulated by miRNAs (miR167 and miR160, respectively).^{17–21} Huang et al.²² have recently characterized the expression of miR160 in *Arabidopsis* wild type ovules together with miR160-driven ARF17 modulation. Mature miR160 was detected not only in the chalaza and funiculus but also within the MMC, and one of its targets (*ARF17*) was shown to be a key determinant for promoting MMC specification.²² Auxin is not the only phytohormone involved in female germline acquisition for a recent study by Cai et al.²³ showed that brassinosteroids biosynthesis and signaling components were also linked to female germline fate acquisition.

The study reported here is focused on the role of ARF10, another miR160 target, in the differentiation of the FM within the ovule. Our interest in this gene stemmed from recent comparative transcriptomic analyses intended to identify apomixis-candidate genes in the aposporous subtropical grass *Paspalum notatum* which revealed that both miR160 and *ARF10* were differentially expressed in the apomictic genotypes.^{24,25} While current literature on *ARF10* function is primarily focused on its activity in germination and somatic embryogenesis, blade outgrowth, leaf/leaflet initiation, and floral organ development,^{21,26–29} the detection of *ARF10* differential expression in flowers of sexual and apomictic *P. notatum* plants at megasporogenesis/megagametogenesis stages suggested an additional role. By establishing the function of the miR160/*ARF10* interaction in *Arabidopsis* sexual reproduction we have attempted to throw light on any role it may play in reproductive development. Our data reveal that strict spatial regulation of *ARF10* by miR160 is required for the induction of a single female germline and, significantly, that ectopic expression of *ARF10* throughout the ovule leads to the emergence of supernumerary FM, either reduced (surviving spores) or unreduced (originated from somatic cells). The formation of these extra FM leads to the development of misoriented, supernumerary, morphologically dissimilar female gametophytes, a phenotype mimicking aposporous apomixis. Furthermore, we also show that the regulation of *ARF10* expression in the nucellus during ovule primordium development is mediated by a combination of (1) transcriptional regulation by the MADS-box transcription factor STK and (2) post-transcriptional control by AGO1 and miR160.

RESULTS

ARF10 expression surrounds the MMC and its meiotic products

To study the expression pattern of *ARF10* in wild type contexts, we used *Arabidopsis* lines expressing an ARF10_GREEN FLUORESCENT PROTEIN (GFP) fusion protein.²¹ No GFP signal was detected at early pre-meiotic stages when ovules are finger-like (stages 2-I, in Hernández-Lagana et al.³⁰). At stage 2-II, when the MMC is clearly differentiated and immediately prior to meiosis, a weak but clear GFP signal was detected in the L1 and L2 layer, surrounding the MMC (Figure 1A). During meiotic divisions, the signal became restricted to a few cells surrounding the dividing MMC and, after meiosis, during the FG1 stage of gametogenesis, it appeared only at the top of the FM and started to be visible in the integuments (Figure S1A). At FG7, after three rounds of mitosis, the GFP signal remained in the outer integuments, being undetectable within the embryo sac (Figure S1B).

To determine *ARF10* expression in the absence of miR160 regulation, we used two *Arabidopsis* lines²¹ in which the miR160-binding site was modified to make *ARF10* insensitive to miR160 regulation, *mARF10_GFP* (*mARF10a* and *mARF10b* - Figures 1B and 1C, respectively,

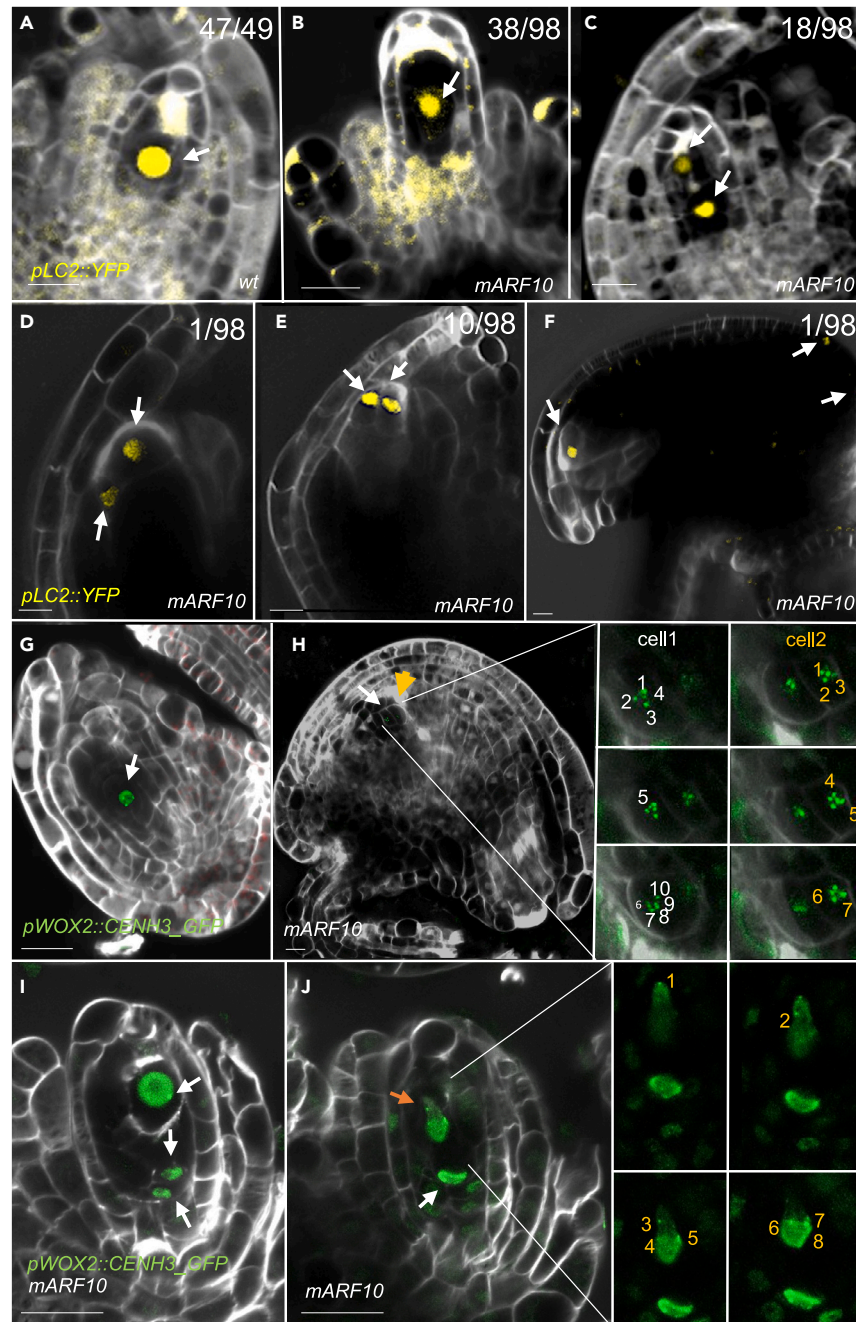


Figure 2. Extra functional megaspores detection in *mARF10* background

(A) *pLC2::YFP* FM identity marker in the wild type background.

(B–F) *pLC2::YFP* in the *mARF10* background: (B) YFP signal detects the functional megaspore, meiosis occurred early with respect to integument development; (C) extra YFP signal detected close to the degenerated megaspores; (D and E) extra YFP signals in the L1 layer; (F) YFP signal in sporophytic tissue at ovule mature stage. The LC2 FM marker signal was counted in a fluorescent microscope and a significance of statistical analysis was performed using 95% Confidence Interval (CI): 48.98% ovules with one functional megaspore ($0.3882 < p < 0.5922$), 19.39% with more than one functional megaspore ($0.1236 < p < 0.2887$) and 31.63% without signal ($0.2281 < p < 0.4191$) ($n = 98$ ovules). In a wild type background, 97.96% ($0.8776 < p < 0.9989$) showed one functional megaspore and 2.04% ($0.0011 < p < 0.1224$) two functional megaspores ($n = 49$).

(G) *pWOX2::CENH3_GFP* in wild type background, showing a single reduced FM with five chromosomes (green dots).

(H) mature ovule with two cells at the chalaza pole expressing the GFP marker (white and yellow arrow, respectively); the cells are non-reduced, as more than five green dots are detected per cell. In the right panels, different focal planes of each one of the cells are shown: 10 chromosomes are visible in cell 1 (white arrow), while 7 in cell 2 (for more details see Video S1).

Figure 2. Continued

(I and J) two different focal planes of the same ovule at FG1 stage: (I) three functional megaspores are detected (white arrows). The upper one display 5 chromosomes (five green dots) (for more details see [Video S2](#)), the bottom ones present more than 5 chromosomes. (J) in a different focal plane of the same ovule, new cells expressing the FM marker are visible: the upper one (yellow arrow) display at least 8 chromosomes (magnified panels at right, full view at [Video S2](#)). Scale bars:10 μ m.

mARF10 stands for mutated *ARF10*. Confocal microscopy analyses revealed a strong GFP signal in the nuclei of all ovule primordia cells. A clear signal was observed just before meiosis - stage 2-II (Hernández-Lagana et al.³⁰), with the fluorochrome being detectable in the whole ovule, even inside the MMC ([Figures 1B and 1C](#)). After meiosis (stage FG1), following FM differentiation, the signal remained visible in all cells ([Figure S1C](#)). During gametogenesis (FG2-FG6), it was particularly visible in all integument layers and in FG7 mature ovules ([Figure S1D](#)), where it was detected in the inner and outer integuments and even within the embryo sac. Taking our findings together with those Huang et al.,²² we conclude that, in wild type plants, *ARF10* is transcribed throughout the ovule from stage FG0 (ovule primordia pre-meiosis) to FG7 (mature ovule), but the concomitant action of miR160 results in its silencing in all cells except for a few cells surrounding the MMC immediately before and during meiosis (from FG0 to FG1), and in the outermost cells of the external integuments at later stages (FG2-FG7).

***mARF10_GFP* lines exhibit supernumerary enlarged cells around the MMC**

We then used the miR160-insensitive *mARF10_GFP* lines²¹ to study the impact of *ARF10* expression repatterning on ovule development and fertility. Inflorescences from *mARF10* lines *a* and *b*, and from wild type plants, were cleared and studied using Differential Interference Contrast (DIC) microscopy. At stage 2-I, FG0 (when the MMC becomes distinguishable from the surrounding nucellar cells owing to its increased size) a significant number of ovules were observed to contain multiple enlarged cells ([Figures 1D–1F](#)). The percentage of ovules with these multiple enlarged cells was 22.5% in *mARF10a* ($n = 23/103$), and 21.6% in *mARF10b* ($n = 44/204$), compared with only 7% in wild type ovules ($n = 21/300$).

To establish the identity of these supernumerary enlarged cells, we crossed the *mARF10* lines with the MMC identity marker *pKNU::nlsYFP*³¹. Confocal analysis showed that, in the wild type context, the signal was clearly central and occupied all the available space ($n = 318$) ([Figure 1G](#)). In the *mARF10* lines, only one cell expressed the YFP signal while the extra enlarged cells displayed no signal ($n = 189/290$) ([Figures 1H and 1I](#)); however, the cell generating the YFP signal was often displaced to the side of the ovule, presumably resulting from the expansion of one or more adjacent cells. YFP signal-counting showed no difference between the wild type and the *mARF10* backgrounds. The commitment of these extra enlarged cells to meiotic entry was assessed using the meiotic precursor *ASY3::RFP*³² ([Figure 1J](#)). In the wild type context, the *ASY3::RFP* signal was detected only within the MMC ([Figure 1J](#)). When this marker line was introgressed in the *mARF10* background, only one cell per ovule, often displaced to the side, expressed the RFP signal ($n = 20/50$) ([Figures 1K and 1L](#)), meaning that only one of the enlarged cells accumulates the meiotic precursor and is capable of entry into meiosis ([Figures 1K and 1L](#)). To further dissect meiotic progression, we have used Renaissance staining, which allows the detection of the callose meiotic septa¹¹ ([Figures 1M–1O](#)). Again, only one cell was found to enter in meiosis ($n = 100$) in the *mARF10* lines, often displaced to the side, when compared to wild-type ovules ($n = 27/100$). No alterations in the pattern of callose deposition around the MMC or in the meiotic septa were visible in the *mARF10* lines. Taken together, these findings are consistent with the fact that only one of the enlarged cells have true MMC identity, since only one cell accumulates the meiotic precursor and forms callose septa, indicating meiotic entry and progression.

Seed set analysis of the two independent lines *mARF10_GFPa* ($n = 350$ ovules) and *mARF10_GFPb* ($n = 186$ ovules) revealed siliques with a significant percentage of unfertilized ovules when compared with wild type ($n = 243$ ovules) (28% for *mARF10a* and 27% for *mARF10b*) ([Figures S2A–S2E](#)). Moreover, the vegetative organs of *mARF10_GFPa* and *mARF10_GFPb* plants showed anomalies previously described by Liu et al.²¹ The most severe phenotype (seen in average in 1/20 plants) resulted in very small and completely sterile plants, i.e., siliques without any fertilized ovules. Other plants displayed more moderate phenotypes, with impaired development, less unfertilized ovules, and serrated leaves. After meiosis, at FG1 stage, *mARF10* DIC analysis also showed extra enlarged cells around the legitimate FM in 25.8% of 348 ovules compared with 0% of 300 ovules in wild type ([Figures S2F–S2H](#)).

***mARF10* lines present apospory-like phenotypes**

To further investigate the identity of the extra enlarged nucellar cells surrounding the FM, we crossed the FM identity marker *pLC2::nlsYFP*³¹ into the *mARF10* lines ([Figures 2A–2F](#)). In the *mARF10* sterile phenotype, only 5% of the ovules expressed the marker ($n = 250$). However, in *mARF10* moderate phenotypes we detected several defects. In a considerable proportion of ovules, meiosis occurred when the integuments were just emerging, and the YFP signal was evident earlier than in wild type, i.e., before the integuments had surrounded the ovule ([Figure 2B](#)). Moreover, extra cells with FM identity appeared around the legitimate FM ([Figures 2C–2F](#)). These cells do not correspond to a 2n gametophyte since cell walls were clearly distinguishable between the marked cells ([Figures 2C–2F](#)). Some of them seem to be extra viable megaspores surviving from meiosis (i.e., they are located within the meiotic tetrad lineage) ([Figure 2C](#)), while others originate from surrounding non-reduced cells (i.e., they appear in the nucellus or the integuments) ([Figures 2D and 2E](#)). At ovule maturity, ectopically located signals were also detected in the integuments ([Figure 2F](#)). In *mARF10* plants, the LC2 marker revealed 49% ovules with one FM, 19% with more than one FM and 32% without signal ($n = 98$). In a wild type background, we counted 98% ovules with canonical development and 2% ovules with altered development (possible evidence of 2 megaspores) ($n = 49$) (see statistical data in the legend of [Figure 2](#)). Our results therefore suggest in *mARF10*

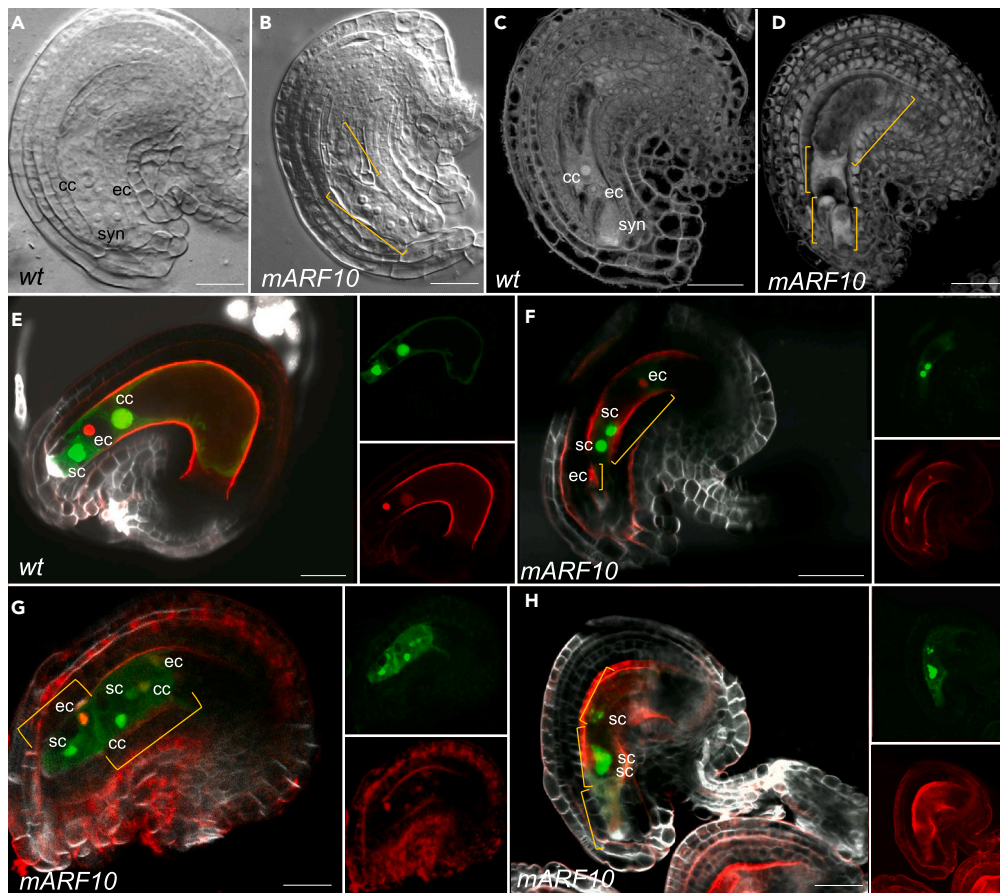


Figure 3. *mARF10* female gametophyte analysis revealed developmental alterations

(A and B) DIC images from wild type and *mARF10* mature ovules, extra numerary nuclei were detected in the *mARF10* mature embryo sacs. (C and D) Feulgen staining of wild type and *mARF10* mature ovules revealed different embryo sac limits when compared with wild type. Yellow bars mark different embryo sacs. (E) Left panel: wild type mature ovule expressing *FGR7.0*; right panel: green and red channels of the same image, two synergids expressing the GFP marker are positioned in the micropillar pole, flanked by the egg cell (RFP red marker) and the central cell (yellowish color given by the red and green channel fusion). (F–H) *mARF10* ovules expressing *FGR7.0*. (F) two egg cells are detected in opposite poles of the embryo sac, and two synergids in the middle region (green and red channels are shown at right); (G) several cells showing synergid/central/egg cell identity. (H) potentially three embryo sacs, in two of them groups of synergid cells are visible. Renaissance staining was used to mark cell walls. Green corresponds to GFP/YFP signal and red to RFP signal. Counting for the *FGR7.0* marker crosses: wt-like ovules: 5; abnormal ovules: 37; ovules without signal: 74 ($n = 116$). For DIC imaging, the significance of statistical analysis was calculated by using 95% Confidence Intervals (CI), as follows: misplaced supernumerary nuclei surrounded by membranes 25% ($0.2112 < p < 0.3022$) ($n = 370$). In WT, no supernumerary nuclei were observed 0% ($0 < p < 0.0158$) ($n = 300$). sc: synergid cells; ec: egg cell; cc: central cell. Scale bars: 20 μ m.

lines there are extra enlarged nucellar cells that express the FM identity marker. By contrast, in pre-meiotic wild type ovules approximately 7% show enlarged cells surrounding the MMC, but they become no longer visible at FG1. To better understand whether these extra FM were reduced or unreduced, we used a second marker, *pWOX2:CENH3_GFP*, which is active specifically in the FM and clearly localized the chromosome centromeres, making it possible to count the number of chromosomes in each cell³³ (Figures 2G–2J). In wild type backgrounds, five chromosomes were detected in the surviving FM after meiosis (Figure 2G). By contrast, in *mARF10* backgrounds we found some cells expressing the *pWOX2:CENH3_GFP* marker that contain more than five chromosomes. From a total of $n = 113$ ovules analyzed, only $n = 17$ showed a clear signal and could be used for counting. Non-reduced cells expressing *pWOX2:CENH3_GFP* were observed after meiosis surrounding the reduced FM, and also in the mature ovule (Figures 2H–2J, video projections S1 and S2). These results suggest that some of the additional FM cells are non-reduced, a phenotype commonly detected in aposporous apomictic species.

***mARF10* lines show gametophytic cell identity defects**

To investigate female gametophyte development at later developmental stages (FG7), we used a combination of clearing and DIC microscopy of emasculated wild type and *mARF10* pistils (Figures 3A and 3B, respectively). In the wild type line, a typical seven celled embryo

sac was always observed ($n = 300$). In *mARF10* lines we observed that 25% of the ovules presented misplaced supernumerary nuclei (Figure 3B, $n = 370$). Through Feulgen staining, we confirmed an abnormal cellular organization within *mARF10* gametophytes, as illustrated in Figures 3C and 3D. Particularly noteworthy are several examples of aberrant development at the embryo sac seen in the *mARF10* lines, which markedly differ from the canonical typical seven-celled embryo sacs observed in the wild type. Additional images of these atypical embryo sacs detected in *mARF10* are shown in Figures S3A–S3E. These aberrant structures may indicate the presence of extra embryo sacs, a characteristic commonly observed in aposporous apomictic species like *Paspalum notatum* (for comparison, a DIC picture is provided) (Figure S3F).

However, it is essential to acknowledge the possibility that these additional cells may indeed belong to the same sac but are showing abnormal identities and positions. To determine whether several embryo sacs were present in the mature ovule and/or if the gametophyte cell-identity was compromised, the FGR7.0 female marker line³⁴ was crossed into the *mARF10_GFP* background. FGR7.0 combines marker genes that label synergid cells, the egg cell, and the central cell with different color (EC1:NLS_3xdsRed for egg cell, DD22:NLS_YFP for central cell/endosperm, and DD2:NLS_3xGFP for synergid cells/endosperm).³⁴ In mature ovules from emasculated wild type flowers, the marker line showed normal embryo sacs (Figure 3E) but some ovules of the *mARF10_GFP* line (Figure 3F) were characterized by supernumerary egg cells situated at different poles of the embryo sac, distant from the correct location. The *mARF10* lines also exhibited embryo sacs with an excessive number of cells, displaying concurrent identities of egg, synergid, and central cells (Figure 3G). Moreover, we also detected embryo sacs expressing only synergid identity at the middle of the sac (Figure 3H). Additional images depicting abnormal sacs with multiple identities and unusual locations can be seen in Figure S3 (Figures S3G–S3O). The presence of cells expressing egg/synergid/central cell markers at abnormal locations suggests either the formation of supernumerary embryo sacs or cell identity misspecification.

As previously indicated, some *mARF10* lines exhibited nearly sterile phenotypes. In these plants the increased presence of enlarged cells before meiosis and the occurrence of aberrant gametophytes were prominent, and these abnormalities appeared to be linked with impaired integument growth, suggesting a potential delay in integument formation (Figures S4A–S4D). More rarely, extreme examples of this defect were seen, where integuments remained undeveloped and gametophytes were directly expelled from the mature ovule or missing, or where an apparent aborted gametophyte was present adjacent to a normal gametophyte (Figures S4D–S4F). Taken together, our findings suggest the presence of one or several misoriented gametophytes with altered cell identity, a phenotype reminiscent of naturally-occurring aposporous apomictic plants.

arf10 defective mutants show aberrant reproductive phenotypes

To gain deeper insights into the involvement of ARF10 in ovule development, we analyzed ovule development in a homozygous line carrying an insertional mutation, designated as *arf10_2*. To confirm the mutation site in the *ARF10* sequence, PCR amplicons were sequenced. The *ARF10* transcript representation was then quantified by qPCR, revealing a relative expression of 0.3 when compared with wild type plants (SD: 0.1569) (Figure S5C). Both cleared *arf10_2* and wild type ovules were examined using DIC microscopy; at ovule pre-meiotic stage 2I some supernumerary enlarged cells were observed, but the numbers were not statistically significant in comparison with wild type (10.8% in *arf10_2* $n = 414$ vs. 8.3% in wild type $n = 336$). Upon further examination of the ovule development, a potential delay in meiosis became evident. Notably, in a considerable proportion of ovules, the linear tetrad degeneration had not occurred by the time integuments enclosed the nucellus — 24.9% in *arf10_2* ($n = 334$ ovules) compared to 0% in the wild type ($n = 315$ ovules) (Figures S5A and S5B). Renaissance staining was then used to follow meiotic progression in these ovules¹¹ (Figures 4A–4H). To simplify statistical analysis, meiosis was divided into three FG stages with respect to integumental development: FG0, which corresponds to finger-like ovule prior to integument growth, FG1-I during which meiosis is taking place and before the ovular enclosure by the integuments and FG1-II, following meiosis when integuments completely enclose the nucellus. As seen in Figures 4A–4D, most wild type ovules entered meiosis at FG0 (74%, $n = 239$ ovules) and FG1-I (25%, $n = 94$ ovules), with meiosis being completed by FG1-II (0%, $n = 145$ ovules). By contrast, the proportion of *arf10_2* ovules entering meiosis at FG0 was 28% ($n = 298$), while at FG1-I was 40% ($n = 55$) and 7% ($n = 57$) completed meiosis by FG1-II (Figures 4E–4H). According to these results, *arf10_2* mutant ovules are delayed in entering meiosis, which extends into stage FG1-II. No alterations in the pattern of callose deposition around the MMC or in the meiotic septa were detected in the *arf10_2* ovules (Figures 4E–4G). To further determine the identity of the cells delayed in meiotic entry, *arf10_2* mutants were crossed with the *pKNU:nlsYFP* MMC marker line.³¹ Strikingly in FG0, 18% displayed signal (Figure 4J, $n = 329$), with 82% of the *arf10_2* ovules showing no signal (Figure 4I, $n = 329$). In a wild type background, ovules with signal occurred in significantly higher numbers (Figure 4K, $n = 318$), pointing to either disruption or delay in the acquisition of MMC fate in the mutant. To further test the hypothesis that meiosis was delayed and probably also the acquisition of MMC identity, based on evidence from the KNU marker, we analyzed *arf10_2* ovules closer to FG1 stage, with elongated integuments. Strikingly, 62% ($n = 117/184$) of the analyzed ovules displayed YFP signal, demonstrating that the acquisition of the identity was delayed as well as meiosis (Figure 4K). Seed set analysis showed a significant increase in the percentage of unfertilized ovules in mutant lines (14%, $n = 792$ ovules) when compared with wild type (1%, $n = 738$ ovules). Homozygous mutants produced only 84% mature seeds, a number significantly lower than wild type (98%) (Figures 4L–4N). Furthermore, we detected a lack of coordination between embryo sac and integument development, since in a substantial number of ovules progression of gametogenesis was delayed, with some ovules arrested at the two-nucleate stage (15.1% for *arf10_2* ovules $n = 396$ and 2.3% for wild type ovules $n = 300$) (Figures 4O–4Q). Complementation tests demonstrated that in three plants of the cross *arf10_2* × *ARF10_GFP*, there were 8% unfertilized ovules ($n = 642$) in average, which is statistically equivalent to the percentages detected in wild type plants. A second defective allele, *arf10_3*, was analyzed and the

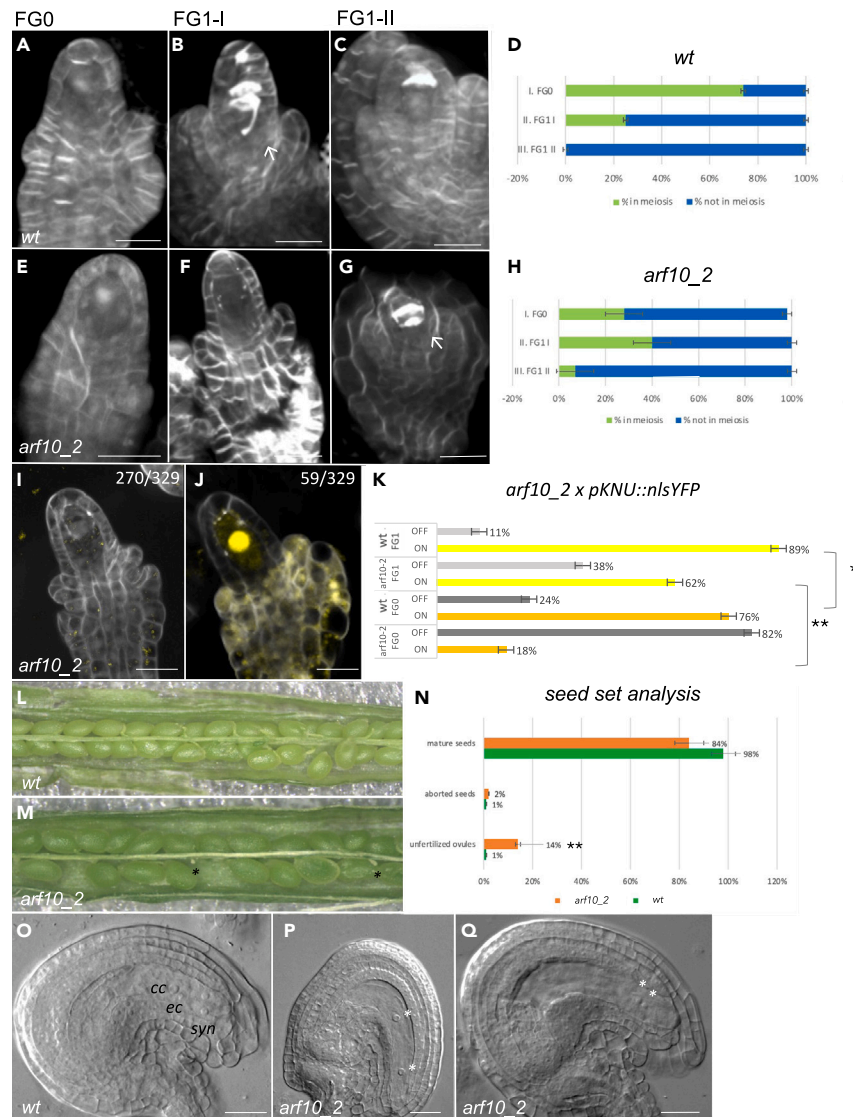


Figure 4. *arf10_2* defective mutant reproductive phenotype shows developmental delay

(A–C) wild type Renaissance staining highlighting meiotic progression at three different ovule stages; (A) FG0, finger-like ovule showing elongating integuments. (B) FG1-I, meiosis ongoing or completed; the integuments have yet to cover the ovule. (C) FG1-II after meiosis, integuments fully elongated, callose accumulation signifies tetrad degeneration. (D) meiosis proportion in Renaissance-stained wild type ovules at three different stages. (E–G) *arf10_2* Renaissance staining highlighting meiotic progression at three different ovule stages (stages as in A–C). Meiosis is still in progress when integuments are fully elongated (white arrow). (H) meiosis proportion in Renaissance-stained *arf10_2* ovules at three different stages. (I and J): *arf10_2* ovules without (I) and with (J) *pKNU::nlsYFP* signal. (K) Bar chart showing *pKNU::nlsYFP* expression in wild type and *arf10_2* backgrounds at FG0 and FG1 stages: ON: YFP expression, OFF: no expression. (L and M) seed set analysis in WT and *arf10_2*, black asterisks mark unfertilized ovules. (N) proportion between mature seeds/aborted seeds/unfertilized ovules. (O–Q) DIC imaging of wild type and *arf10_2* mature ovules. Some *arf10_2* ovules presented a block during gametogenesis; white asterisks indicate nuclei. The significance of differences between wild type and mutants for seed set and *pKNU::YFP* signal detection was evaluated by the Student's t test (** $p < 0.05$; *** $p < 0.001$). For DIC imaging, the significance of statistical analyses was evaluated using the 95% Confidence Interval (CI): 15.15% vs. 2.33%; $n = 396$ and 300; 95% CI: $0.1184 < p < 0.1915$ and $0.0102 < p < 0.0495$ for *arf10_2* and the wild type, respectively, Data are represented as mean \pm SEM; scale bars: 20 μm ; cc: central cell; ec: egg cell; syn: synergid cells.

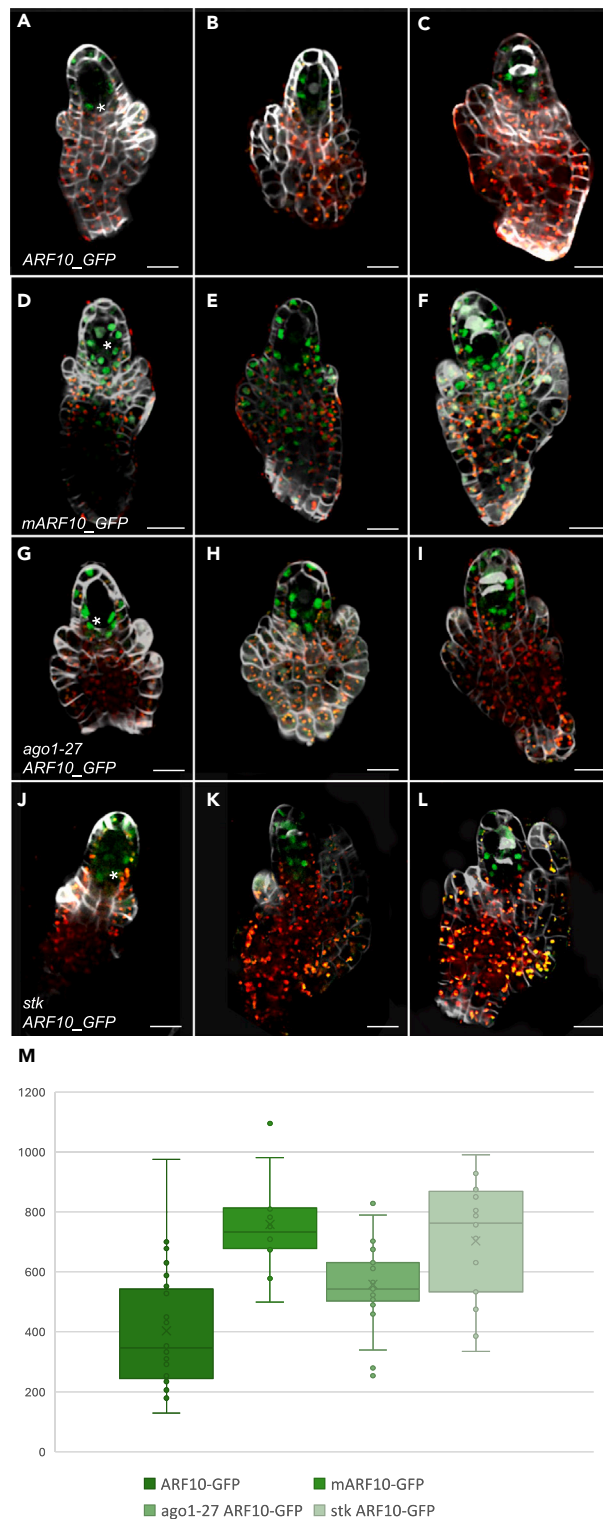


Figure 5. ARF10 expression patterns in different genetic contexts

(A and B) In wild type context, *ARF10_GFP* expression at pre-meiosis is detected in a few cells surrounding the MMC. (C) in the post-meiotic ovule, *ARF10_GFP* expression is maintained in few L2 cells surrounding the meiocytes. (D and E) *mARF10_GFP* expression pattern at pre-meiosis, a strong GFP signal is detected in all ovule cells, including the MMC. (F) *mARF10_GFP* expression at post-meiosis, the GFP signal is detected in all ovule cells, including the funiculus and chalaza.

Figure 5. Continued

(G–I) *ARF10_GFP* protein accumulation in *ago1-27* nucellar cells at three successive developmental stages, from MMC differentiation to meiosis. The expression is observed in the same domain as for the wild type context, but the signal is stronger (see quantification).

(J–L) *ARF10_GFP* protein accumulation in *stk* nucellar cells at three successive developmental stages, from MMC differentiation to meiosis. The expression is observed in the same domain as for the wild type context, but an increased signal is detected within the MMC. The signal is stronger (see quantification).

(M) mean GFP intensity detected in the nucellus for the different genotypes: *mARF10*, *ago1* and *stk* backgrounds showed significantly higher signal levels with respect to wild type ones. Data are represented in a dot plot as mean \pm SEM. Statistical analysis using one-way ANOVA and Tukey's HSD test ($p < 0.01$) showed significant differences in GFP expression levels between WT and *mARF10*, *ago1-27 ARF10_GFP*, and *stk ARF10_GFP*. Scale bars: 20 μ m. Cell walls were stained using Renaissance. Green signal corresponds to GFP.

main phenotypes described above were confirmed (Figure S6G). Seed set was also compromised, as 21% of the ovules were unfertilized and an arrest in seed development was detected in 14% of the seeds ($n = 831$) in comparison with wild type plants, which presented only 5% unfertilized ovules and 1% of arrested seeds ($n = 738$) (Figures S5D–S5F). To confirm the mutation site in *ARF10*, PCR amplicons were sequenced and *ARF10* transcript representation was quantified by qPCR. No expression was detected in the mutant (Figure S5G). A delay in entering meiosis was observed in 63% of the analyzed ovules ($n = 305$) which was partially reflected in a block of gametogenesis in 30% ($n = 430$), mainly at two-nucleate stage (Figures S5H and S5I). Taken together, these data indicate that, in the wild type, *ARF10* expression in cells surrounding the MMC, and subsequently in the external integuments, is required for correct initiation of meiosis and progression of megagametogenesis.

ARGONAUTE 1 and SEEDSTICK regulate ARF10 nucellar silencing

To explore the mechanism underlying miR160-mediated *ARF10* silencing, we attempted to identify the ARGONAUTE protein associated with this process. We first hypothesized that AGO1 played a role, since *AGO1* transcripts had been reported as differentially expressed in pre-meiotic spikelets of aposporous apomictic and sexual *Paspalum* plants.²⁵ Null alleles of *AGO1* cause early lethality, so we analyzed a previously described viable but hypomorphic allele of *ago1-27*³⁵ known to be defective in the RNaseH-like PIWI domain, which is involved in mRNA cleavage and translational repression.³⁶

We first conducted an analysis of *ARF10* expression in both wild type and *ago1-27* backgrounds. In wild type samples (Figures 5A–5C), *ARF10* exhibited expression primarily around the MMC, within the L1 and L2 layers, as mentioned before. Contrastingly, in backgrounds displaying miR160 insensitivity (*mARF10_GFP*) (Figures 5D–5F), expression was widespread throughout the ovule. Notably, in *ago1-27* pre-meiotic/meiotic nucellar cells, a pronounced expression of *ARF10* was observed within the nucellus (Figures 5G–5I), while no expression was detected in the MMC and chalaza.

GFP intensity variation among the different lines was quantified using *ImageJ* software, focusing exclusively on nucellar cells. Statistical analysis uncovered disparities in GFP intensity between *ARF10_GFP* and *mARF10_GFP* (Figure 5M). Significant differences were also observed between *ARF10_GFP* and *ago1-27 ARF10_GFP*, indicating a role for AGO1 in the nucellar regulation of *ARF10* (Figure 5M). To better explore the connection between AGO1 and *ARF10*, we analyzed the phenotype of *ago1-27* mutants during the early stages of ovule development. Approximately 25% ($n = 203$) of the ovules from *ago1-27* mutants exhibited multiple enlarged cells during pre-meiotic stages, compared to only 4% ($n = 435$) in wild type samples. This observed phenotype bears a remarkable similarity to that observed in *mARF10* lines. To further investigate potential disruptions in female gametophyte formation, we crossed *ago1-27* with the *FGR 7.0* marker (Figure S6). Mature *ago1-27* ovules resulting from these crosses exhibited similar phenotypes to those observed in *mARF10* lines (see Figures S6D–S6G). Notably, in many of these ovules, the positioning of the egg cell was significantly altered, being often found near the chalazal pole rather than the micropylar pole. Moreover, both synergid and central cells were frequently found to be misplaced - as seen for *mARF10* in some cases.

Concurrently, we initiated a series of experiments aimed at unraveling the intricacies of STK regulation of *ARF10*, as STK has been shown to be involved in female germline development.¹¹ To explore the relationship between STK, miR160 and *ARF10*, we examined *ARF10* expression patterns in crosses between *ARF10_GFP* and *stk-2* lines.³⁷ As was observed in the *ago1* background, in the *stk* mutant *ARF10* was highly expressed in the nucellus (L1 and L2 layers), but in this case we detected an increment of the signal within the MMC during premeiotic/meiotic stages (Figures 5J–5L). This differential expression was confirmed by GFP quantification (Figure 5M). We also conducted chromatin immunoprecipitation (ChIP) followed by qPCR on *pSTK:STK_GFP* plants³⁸ to explore the potential direct control of *ARF10* expression by STK. Analysis of the *ARF10* promoter region (2 kb upstream of the ATG starting site) revealed the presence of six possible STK binding sites, known as CARG boxes³⁹ (Figure S7H). ChIP-qPCR results demonstrated that STK directly binds to the promoter region of *ARF10* via CARG boxes 1 and 2 (Figure S6H), suggesting a direct repression of *ARF10* expression by STK.

As STK was previously shown to be involved in the RNA directed DNA methylation (RdDM) pathway,¹¹ we also investigated the possibility of a methylation control by performing Methylation Content Sensitive Enzyme ddRAD (MCSeEd) analysis⁴⁰ in wild type plants versus *stk* mutants. Triplicate flower samples (up to and including stage¹¹) were collected to minimize the impact of epigenetic variation between individuals.^{41,42} Eighteen (18) MCSeEd libraries were constructed by double restriction-ligations, using *MseI* in combination with one of three methylation-sensitive enzymes *Acil*, *PstI*, and *EcoT22I* for CG, CHG, and CHH contexts, respectively (Table S1). Exclusively mapped loci (MCSeEd loci) were normalized, filtered, and then analyzed with MethylKit to infer the number of differentially methylated positions (DMPs) between mutants and wild type plants, as either delta positive or delta negative. A total of 1,507 DMRs were scored in the *stk* mutants compared with the wild type plants (Table S1). The genomic location of each DMR was mapped onto

Arabidopsis transcribed genic regions extended by 2.5 kb at both ends (extended gene bodies; EGBs, Table S2), and the genes belonging to these EGBs were defined as differentially methylated genes (DMGs). The list of DMGs included a CHH-DMR with negative delta methylation that intersected miR160 b at 109 bp from the Transcription Termination Site (TTS), while no methylation differences were encountered for the *ARF10* genomic locus. To validate the differential methylation of the miR160-CHH-DMR, we employed the quantitative (q)MRE technique and, as expected, the digested samples of *stk* mutants showed a value lower than the wild-type ones, demonstrating that the positions belonging to the miR160-CHH-DMR were demethylated (Figure S6J; Table S3). Following this, we investigated whether STK influences the expression of miR160. We did a stem loop-PCR to quantify the levels of mature miRNA in the *stk* mutant background, revealing a significant downregulation of the mature form of miR160 (Figure S6I). Altogether, our findings suggest that STK may modulate *ARF10* levels through two distinct mechanisms: (1) a direct negative regulation mechanism involving STK binding to the *ARF10* promoter and (2) an indirect process involving methylation of the miR160b genomic locus, resulting in increased mature miR160 levels and subsequent *ARF10* repression.

To investigate into cellular dynamics with greater precision, prompted by the distinct GFP pattern, we utilized both sense and antisense GFP probes via *in situ* hybridization. This approach enabled us to explore transcript accumulation at the cellular level in these lines. At premeiosis stages, a faint signal was detected across the ovule in *ARF10_GFP* lines (Figure S7A). However, in *mARF10_GFP* lines (Figure S7B) the accumulation of transcripts within the ovule was notably higher. Additionally, when comparing hybridization of *ARF10_GFP* with *ago1-27 ARF10_GFP* and *stk ARF10_GFP*, the signal was higher, but lower than that observed with *mARF10_GFP* (Figures S7C and S7D). In *stk*, a lower GFP hybridization signal was also detected within the MMC. In conclusion, the observed transcript levels suggest that both AGO1 and STK play roles in suppressing *ARF10* expression within the nucellar layers, although their impact on transcript abundance appears to be minor. Conversely, in *mARF10*, the regulation by miR160 appears to have a significant impact, affecting transcript abundance in the nucellus, chalaza, and funiculus. It is noteworthy that transcripts were detected throughout the ovule rather than being confined to a specific cell type, suggesting potential involvement of post-transcriptional/translational mechanisms in *ARF10* regulation. Finally, we tested the abundance of miR160 mature RNA by *in situ* hybridization, as demonstrated in Figure S8. In WT ovules, miR160 is distributed throughout the ovule primordia cells, except for the cells surrounding the MMC (Figure S8A). In *stk* mutants, the miR160 signal was markedly lower within the MMC (Figure S8B), suggesting that STK positively regulates miR160 expression, which agrees with the GFP hybridizations. Analysis of *ago-1* mutants (Figure S8C) did not show a significant difference compared to the WT, indicating that AGO1 does not influence miR160 expression levels.

DISCUSSION

Does *ARF10* control a gametophytic factor?

This study highlights the critical role of *ARF10* during the regulation of gene expression in response to the plant hormone auxin. Our findings underscore the essential contribution of *ARF10* to the development of both sexual and asexual female germlines. In a sexual wild-type plant, such as the model *Arabidopsis*, during the early stages of ovule development, we observed a highly specific expression pattern of *ARF10* localized within the ovule nucellus, surrounding the MMC—the cell destined to undergo meiosis. Previous studies have demonstrated that *ARF10* is regulated by miR160,²¹ but here we have analyzed the detailed dynamics of this regulation within the ovule, particularly in lines where *ARF10* was insensitive to miR160 regulation (*mARF10*). GFP signal comparisons between *ARF10-GFP* and *mARF10-GFP* lines revealed that *ARF10* transcription occurs ubiquitously across the ovule during all stages of development, but the expression is subsequently silenced by miR160 in most cells, except for those surrounding the MMC. Consequently, during the ovule primordia stage, the MMC appeared to be the only cell enveloped by *ARF10*-expressing cells.

The ectopic expression of *ARF10* identified in the *mARF10* lines induces a highly specific phenotype during ovule development: the emergence of multiple enlarged cells surrounding the MMC, lacking MMC identity initially but ultimately acquiring FM characteristics. As demonstrated through crosses with the FM-identity markers *pLC2:nlSYFP* and *pWOX2:CENH3_GFP*, in *mARF10* lines, the additional enlarged cells originating from nucellar and integumental layers exhibit FM identity signal. Some of them presented a non-reduced status, characterized by possessing more than five chromosomes, while others were reduced, resulting directly from the meiotic events. Supernumerary surviving reduced megaspores that acquire an FM identity were also detected. At later developmental stages, we identified misoriented embryo sacs with anomalous morphology. A similar phenotype including the emergence of supernumerary reduced and unreduced FMs was recently reported in *trimethylguanosine synthase 1* defective lines by Siena et al. (2023).⁴³ Moreover, supernumerary reduced FM are also formed in *Arabidopsis* plants carrying loss-of-function mutations in the miR822.⁴⁴

In the absence of *ARF10* within the ovule in *arf10* mutants, the progression of meiotic entry is compromised. Morphological identification of defective meiotic entry was achieved by staining division septa with the Renaissance stain, while observing the correlation between division progression and integument size. This observation was associated with the delay in the establishment of MMC identity, as revealed by the MMC marker *pKNU:nlSYFP*. The challenges observed in meiotic entry directly affect ovule development, resulting in arrest at the gametogenesis (FG2 stage) in a significant number of ovules, leading to abortion. The partial penetrance of this effect hints at the potential redundancy of *ARF10* with another ARF, possibly *ARF16*, as indicated by Wójcick et al.²⁶ Taking these findings into account collectively, we suggest that *ARF10* plays a functional role in initiating the commitment to gametophyte formation. This process likely occurs before the acquisition of MMC identity, suggesting that early gametophyte commitment serves as a crucial checkpoint preceding reductional division entry. Since *ARF10* is a transcriptional repressor, it is likely to be involved in the suppression of a repressor, allowing the release of a gametophytic signal of unknown nature to the MMC, inducing thereby a primary commitment

to a gametophytic identity in a non-cell autonomous manner. This interpretation is further reinforced by the fact that the ectopic expression of *ARF10* throughout the nucellus (in *mARF10*, *stk* and *ago1* lines), which disrupts the *ARF10* signal, fails to cause the development of multiple MMCs entering meiosis, but rather the emergence of supernumerary enlarged cells with FM identity, able to start gametogenesis. Recently, Huang et al.²² stated that *pARF10:mARF10* and *pARF16:mARF16*, in contrast to *pARF17:mARF17*, fail to produce supernumerary MMC-like cells. Here, we confirmed the absence of legitimate supernumerary MMCs (cells expressing *pKNU-Venus*) in *pARF10:mARF10* lines, but detected extra enlarged cells in the nucellus at pre-meiosis. However, any direct comparison between these two sets of results is necessarily complicated by the fact that different *pARF10:mARF10* constructs were employed in the analyses (i.e., the mutated sites were different), and they were introduced in different genetic backgrounds (Ler vs. Col). Moreover, it is a well-known fact that environmental conditions influence the rate of formation of non-reduced FM in aposporous plants, which can have an effect on the detection of the phenotype.

ARF10 regulation in ovule nucellus is complex

Our data unveil a complex regulatory network governing *ARF10* within the ovule primordia nucellus. This regulation involves components such as *miR160*, *AGO1*, and the MADS-box transcription factor *STK*. When *ARF10* is active, it is primarily expressed in a single cell layer surrounding the MMC, detected in the L1 and L2 nucellus layers. In the absence of *AGO1* or *STK* (in *ago1-27 ARF10-GFP* and *stk ARF10-GFP* mutants, respectively), *ARF10* exhibits higher expression levels in the ovule primordia nucella with respect to WT *ARF10-GFP*. Furthermore, in *stk* mutants, a lower GFP signal is detected within the MMC, which is not observed in the *ago-1* mutant background. However, when *ARF10* is rendered insensitive to *miR160* regulation (*mARF10*), its expression becomes ubiquitous, present in the MMC, as well as in all nucellar and chalazal cells. Thus, *ARF10* appears to be transcribed in all ovule cells but silenced in the MMC, the chalaza, and part of the nucellar cells through a mechanism involving *miR160*.

Furthermore, of particular interest is the direct regulation of *ARF10* in the ovule primordia nucellus, which implies the existence of a complex mechanism likely orchestrated by the MADS box transcription factor *STK* and *AGO1*. Notably, our discovery reveals that *STK* can directly bind to the genomic region of *ARF10*, possibly repressing its expression. What is most intriguing is that in the nucellus, this repression operates in a dosage-dependent manner, as evidenced by our findings that *ARF10* expression is higher in *stk* mutants, as observed through GFP quantification and *in situ* hybridization analysis. *STK* has been observed to interact with the RdDM pathway,¹¹ prompting us to investigate whether it could potentially influence not only *ARF10* but also *miR160* expression through this epigenetic pathway. Previous studies have demonstrated that mutants within this pathway exhibit phenotypes associated with female germline fate acquisition, similar to what was described here for *ARF10*.¹⁰ To explore this further, we analyzed the methylation landscape of *stk* mutants compared to wild-type plants. We found that while the *ARF10* locus remained unaffected, the *miR160b* locus displayed differential methylation. This discrepancy in the methylation (hypomethylation) status directly impacted *miR160* expression levels, as evidenced by our quantification of mature *miR160* using stem-loop PCR, which revealed a significant reduction in *stk* mutant backgrounds. We hypothesize that the regulation of *ARF10* is intricately managed by *STK*, exerting masterful control through two distinct avenues: direct binding to its genomic region and indirect modulation via the RdDM pathway (methylation), which regulates the abundance of *miR160* and consequently impacts *ARF10* levels.

Another critical aspect of this puzzle involves *AGO1*. Its absence also results in an elevated expression of *ARF10* in the ovule primordia nucelli, rather than a change in the spatial distribution. Considering the expression pattern of *miR160*, predominantly in the chalaza and funiculus, but also active in the ovule nucelli, we infer that mature *miR160* likely has the ability to travel and silence its targets within the nucellus. This leads to the conclusion that *AGO1* is the *AGO* protein facilitating the silencing of *ARF10* in conjunction with *miR160* in this context. Our findings underscore the previously documented specificity of *AGO*-mediated silencing. Specifically, *AGO1* appears to regulate *ARF10* processing exclusively in the nucellus, while not exhibiting such control in the chalaza or the MMC, where *miR160* may be linked with other family members.

A model for the control of early female reproductive development

Based on the data provided here and elsewhere on *miR160*,²² *AGO1*,⁴⁵ and *STK*³⁸ on ovule expression domains, we propose a model for the *STK*-*miR160/AGO1* control of *ARF10* expression in female reproductive development (Figure 6). During *Arabidopsis* sexual wild type development, at late pre-meiosis (FG0), *ARF10* is silenced by the action of *miR160*, *STK* and *AGO1* in the nucellus (Figure 6A). Meanwhile, *ARF10* accumulates in a restricted ring of L1/L2 nucellar cells surrounding the MMC. From this location, *ARF10* induces the capacity for future gametophyte formation in the MMC cell and acts as a checkpoint for full MMC identity acquisition and progression into meiosis (Figure 6A). This *ARF10* expression domain is maintained around the products of meiosis and is later relegated to the outer layer of the external integuments, where it may be necessary to promote normal gametophyte progression. In *mARF10* lines, there is an increase of *ARF10* levels in the nucellus, and an ectopic expression in the chalaza/funiculus and the MMC (Figure 6B), which induces: (1) an MMC premature entry into meiosis (note that the MMC is the only cell that accumulates meiotic precursors like *ASY3*) and (2) a commitment to form gametophytes from other nucellar cells (somatic). Both aspects of the reproductive phenotype might be related to the particularly high and generalized expression pattern of *mARF10* in *mARF10* lines, since numerous cells in the nucellus are surrounded by others expressing *ARF10*. Therefore, *ARF10* expression possibly influences other nucellar cells, besides the MMC. However, since somatic nucellar cells fail to express other factors required for MMC identity and meiotic entry (perhaps elements of the THO/TREX complex/*TAS3/ARF3*, *ARF17* or the *RBR1* pathways), or even *ASY3* meiotic precursors, they do not undergo megasporogenesis but bypass meiosis, acquire FM identity, and proceed directly into megagametogenesis.

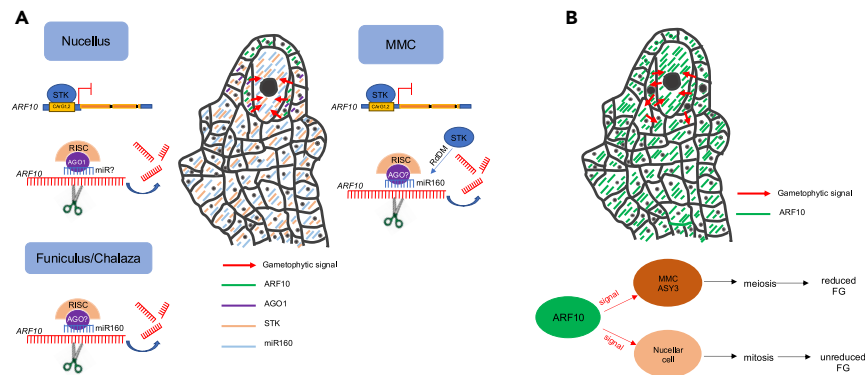


Figure 6. A proposed model for ARF10 function in the ovule

(A) In wild-type pre-meiotic ovule nucellus, *ARF10* is partially and selectively silenced by STK in both the MMC and nucellus cells. STK binds to the genomic DNA at CARG boxes 1 and 2, repressing *ARF10* expression. In the MMC, STK can also induce the expression of *miR160* via the RdDM pathway. *miR160* subsequently silences *ARF10* in collaboration with an AGO protein of unknown identity. In the nucellus cells, AGO1 silences *ARF10* in association with an unidentified miRNA. The regulation of *ARF10* expression in the funiculus and chalaza regions involves *miR160* in conjunction with an unknown AGO protein.

(B) In *mARF10* lines, *ARF10* is ectopically expressed in the nucellus cells, MMC, and funiculus/chalaza cells. This ectopic expression in the nucellus and MMC results in the widespread commitment of additional cells to form gametophytes. However, only the cell that accumulates meiotic precursors, such as *ASY3* (i.e., the MMC), will undergo meiosis (sexual pathway), leading to the formation of a reduced female gametophyte. The generation of additional functional megaspores from somatic companion cells (non-reduced) eventually results in the development of supernumerary, anomalous gametophytes, similar to those observed in aposporous apomictic plants. Black dots represent the cell nuclei, question marks indicate unknown identity.

Conclusions

Here we present evidence that *miR160* restricts the expression of *ARF10* mainly to few cells around the MMC at pre-meiosis. *ARF10* influences the entrance of the MMC into meiosis, by inducing commitment to form a gametophyte. Later, *ARF10* appears to be implicated in the specification of megagametogenesis. Our experiments also indicate that the control of *ARF10* by *miR160* in the nucellus is mediated by AGO1, STK and RdDM. A higher accumulation of *ARF10* in nucellar cells and the MMC induces phenotypes mimicking apospory (i.e., multiple non-reduced embryo sac formation with random orientation of cell-identity types and unusual embryo sac morphology). This study reveals a key mechanism involved in the germline fate acquisition in plant ovules and identifies a potential avenue for the development of molecular strategies for the induction of apomixis in sexual crop species – a long time target of the crop development industry. Considering that in natural apomicts like *Paspalum notatum*, *ARF10* is overexpressed in florets at pre-meiosis and down-regulated during megagametogenesis,²⁵ we speculate that full recreation of the apospory phenotype might require a more specific temporal control.

Limitations of the study

Current microscopy technologies, such as DIG or Feulgen confocal microscopy, do not allow for a conclusive assessment of the embryo sac border location in ovules carrying multiple megagametophytes. In the future, the development of markers that better reveal these limits might facilitate the identification of apospory-like phenotypes. Further experiments, such as Y1H or EMSA, should be conducted to confirm the repression of *ARF10* by STK. Moreover, high-resolution *in situ* RNA sequencing will improve the definition of gene expression boundaries and refine the model presented here.

RESOURCE AVAILABILITY

Lead contact

Further information and requests for resources and reagents should be directed to and will be fulfilled by the lead contact, Marta Mendes (marta.mendes@unimi.it).

Materials availability

This paper analyzes existing, publicly available plant materials (i.e., it did not generate new unique lines). The crosses between these materials are available from the [lead contact](#) upon request.

Data and code availability

- McSeED sequencing data is available at NCBI Database: PRJNA750614.
- Pipeline for methylation analysis from raw reads to DMR identification (<https://bitbucket.org/capemaster/mcseed/src/master/>).
- Any additional information required to reanalyze the data reported in this paper is available from the [lead contact](#) upon request.

ACKNOWLEDGMENTS

The project leading to this work has received funding from the European Union's Horizon 2020 research and innovation programme under the Marie Skłodowska-Curie grant agreement No [645674], Project PROCROP and [872417], Project MAD; Agencia Nacional de Promoción Científica y Tecnológica, Argentina, Project PICT-2019-03414; Universidad Nacional de Rosario (UNR), Argentina, Project: 80020190300021UR; MAE, Italy/CONICET, Argentina cooperation project MAECI AR21GR03. Imaging analyses were carried out at NOLIMITS, an advanced imaging facility established by the University of Milan.

AUTHOR CONTRIBUTIONS

Conceptualization, S.P. and M.A.M.; Investigation, S.P., M.C., C.C., E.C., D.P., M.D.M., G.C.T., R.P., C.M., C.A., M.P., G.M, E.A., and M.A.M.; Methodology, S.P. and M.A.M.; Resources and Data Curation, M.P., E.A., and G.M.; Visualization: S.P., M.C., and M.A.M.; Writing – Original Draft, S.P. and M.A.M.; Writing – Review and Editing, S.P., E.A., H.D., L.C., and M.A.M.; Funding Acquisition, S.P., L.C., and M.A.M.; Supervision: H.D., L.C., and M.A.M.

DECLARATION OF INTERESTS

The authors declare no competing interests.

STAR★METHODS

Detailed methods are provided in the online version of this paper and include the following:

- **KEY RESOURCES TABLE**
- **EXPERIMENTAL MODEL AND STUDY PARTICIPANT DETAILS**
 - Plant material
- **METHOD DETAILS**
 - Genotyping of *arf10* defective mutants
 - Microscopy
 - DNA methylation analysis
 - Silique analysis
 - qPCR analysis
 - *In situ* hybridization
 - Chromatin immunoprecipitation assay followed by qRT-PCR (ChIP qPCR)
- **QUANTIFICATION AND STATISTICAL ANALYSIS**
 - Statistical analyses of proportions

SUPPLEMENTAL INFORMATION

Supplemental information can be found online at <https://doi.org/10.1016/j.isci.2024.111115>.

Received: April 18, 2023

Revised: April 1, 2024

Accepted: October 3, 2024

Published: October 9, 2024

REFERENCES

1. Nogler, G.A. (1984). Gametophytic apomixis. In *Embryology of Angiosperms*, B.M. Johri, ed. (Springer-Verlag), pp. 475–518.
2. Koltunow, A.M., and Grossniklaus, U. (2003). Apomixis: a developmental perspective. *Annu. Rev. Plant Biol.* 54, 547–574. <https://doi.org/10.1146/annurev-arplant.54.110901.160842>.
3. Hand, M.L., and Koltunow, A.M.G. (2014). The genetic control of apomixis: asexual seed formation. *Genetics* 197, 441–450. <https://doi.org/10.1534/genetics.114.163105>.
4. Hojsgaard, D., Klatt, S., Baier, R., Carman, J.G., and Hörandl, E. (2014). Taxonomy and biogeography of apomixis in angiosperms and associated biodiversity characteristics. *Crit. Rev. Plant Sci.* 33, 414–427. <https://doi.org/10.1080/07352689.2014.898488>.
5. Crane, C.F. (2001). Classification of apomictic mechanisms. In *The Flowering of Apomixis: From Mechanisms to Genetic Engineering*, Y. Savidan, J.G. Carman, and T. Dresselhaus, eds. (CIMMYT, IRD, European Commission DG VI FAIR), pp. 24–43.
6. Pinto, S.C., Mendes, M.A., Coimbra, S., and Tucker, M.R. (2019). Revisiting the female germline and its expanding toolbox. *Trends Plant Sci.* 24, 455–467. <https://doi.org/10.1016/j.tplants.2019.02.003>.
7. Petrella, R., Caselli, F., Roig-Villanova, I., Vignati, V., Chiara, M., Ezquer, I., Tadini, L., Kater, M.M., and Gregis, V. (2020). BPC transcription factors and a Polycomb Group protein confine the expression of the ovule identity gene SEEDSTICK in *Arabidopsis*. *Plant J.* 102, 582–599. <https://doi.org/10.1111/tpj.14673>.
8. Hater, F., Nakel, T., and Groß-Hardt, R. (2020). Reproductive Multitasking: The Female Gametophyte. *Annu. Rev. Plant Biol.* 71, 517–546. <https://doi.org/10.1146/annurev-arplant-081519-035943>.
9. Yu, S.X., Jiang, Y.T., and Lin, W.H. (2022). Ovule initiation: the essential step controlling offspring number in *Arabidopsis*. *J. Integr. Plant Biol.* 64, 1469–1486. <https://doi.org/10.1111/jipb.13314>.
10. Olmedo-Monfil, V., Durán-Figueroa, N., Arteaga-Vázquez, M., Demesa-Arévalo, E., Autran, D., Grimanelli, D., Slotkin, R.K., Martienssen, R.A., and Vielle-Calzada, J.-P. (2010). Control of female gamete formation by a small RNA pathway in *Arabidopsis*. *Nature* 464, 628–632. <https://doi.org/10.1038/nature08828>.
11. Mendes, M.A., Petrella, R., Cucinotta, M., Vignati, E., Gatti, S., Pinto, S.C., Bird, D.C., Gregis, V., Dickinson, H., Tucker, M.R., and Colombo, L. (2020). The RNA-dependent DNA methylation pathway is required to restrict SPOROCTELESS/NOZZLE expression to specify a single female germ cell precursor in *Arabidopsis*. *Development* 147, dev194274. <https://doi.org/10.1242/dev.194274>.
12. Benková, E., Michniewicz, M., Sauer, M., Teichmann, T., Seifertová, D., Jürgens, G., and Friml, J. (2003). Local, efflux-dependent auxin gradients as a common module for plant organ formation. *Cell* 115, 591–602. [https://doi.org/10.1016/s0092-8674\(03\)00924-3](https://doi.org/10.1016/s0092-8674(03)00924-3).
13. Ceccato, L., Masiero, S., Sinha Roy, D., Bencivenga, S., Roig-Villanova, I., Ditegou, F.A., Palme, K., Simon, R., and Colombo, L. (2013). Maternal control of PIN1 is required for female gametophyte development in *Arabidopsis*. *PLoS One* 8, e66148. <https://doi.org/10.1371/journal.pone.0066148>.
14. Li, S.-B., Xie, Z.-Z., Hu, C.G., and Zhang, J.-Z. (2016). A review of auxin response factors (ARFs) in plants. *Front. Plant Sci.* 7, 47. <https://doi.org/10.3389/fpls.2016.00047>.

15. Cucinotta, M., Cavalleri, A., Guazzotti, A., Astori, C., Manrique, S., Bombarely, A., Oliveto, S., Biffo, S., Weijers, D., Kater, M.M., and Colombo, L. (2021). Alternative splicing generates a MONOPTEROS isoform required for ovule development. *Curr. Biol.* 31, 892–899.e3. <https://doi.org/10.1016/j.cub.2020.11.026>.
16. Su, Z., Zhao, L., Zhao, Y., Li, S., Won, S., Cai, H., Wang, L., Li, Z., Chen, P., Qin, Y., and Chen, X. (2017). The THO complex non-cell-autonomously represses female germline specification through the TAS3-ARF3 module. *Curr. Biol.* 27, 1597–1609.e2. <https://doi.org/10.1016/j.cub.2017.05.021>.
17. Mallory, A.C., Bartel, D.P., and Bartel, B. (2005). MicroRNA-directed regulation of *Arabidopsis* AUXIN RESPONSE FACTOR 17 is essential for proper development and modulates expression of early auxin response genes. *Plant Cell* 17, 1360–1375. <https://doi.org/10.1105/tpc.105.031716>.
18. Wang, J.W., Wang, L.J., Mao, Y.B., Cai, W.J., Xue, H.W., and Chen, X.Y. (2005). Control of root cap formation by MicroRNA-targeted auxin response factors in *Arabidopsis*. *Plant Cell* 17, 2204–2216. <https://doi.org/10.1105/tpc.105.033076>.
19. Yang, J.H., Han, S.J., Yoon, E.K., and Lee, W.S. (2006). Evidence of an auxin signal pathway, microRNA167-ARF8-GH3, and its response to exogenous auxin in cultured rice cells. *Nucleic Acids Res.* 34, 1892–1899. <https://doi.org/10.1093/nar/gkl118>.
20. Wu, M.F., Tian, Q., and Reed, J.W. (2006). *Arabidopsis* microRNA167 controls patterns of ARF6 and ARF8 expression, and regulates both female and male reproduction. *Development* 133, 4211–4218. <https://doi.org/10.1242/dev.02602>.
21. Liu, P.-P., Montgomery, T.A., Fahlgren, N., Kasschau, K.D., Nonogaki, H., and Carrington, J.C. (2007). Repression of AUXIN RESPONSE FACTOR10 by microRNA160 is critical for seed germination and post-germination stages. *Plant J.* 52, 133–146. <https://doi.org/10.1111/j.1365-313X.2007.03218.x>.
22. Huang, J., Zhao, L., Malik, S., Gentile, B.R., Xiong, V., Arazi, T., Owen, H.A., Friml, J., and Zhao, D. (2022). Specification of female germline by microRNA orchestrated auxin signaling in *Arabidopsis*. *Nat. Commun.* 13, 6960. <https://doi.org/10.1038/s41467-022-34723-6>.
23. Cai, H., Liu, L., Huang, Y., Zhu, W., Qi, J., Xi, X., Aslam, M., Dresselhaus, T., and Qin, Y. (2022). Brassinosteroid signaling regulates female germline specification in *Arabidopsis*. *Curr. Biol.* 32, 1102–1114.e5. <https://doi.org/10.1016/j.cub.2022.01.022>.
24. Ortiz, J.P.A., Leblanc, O., Rohr, C., Grisolia, M., Siena, L.A., Podio, M., Colono, C., Azzaro, C., and Pessino, S.C. (2019). Small RNA-seq reveals novel regulatory components for apomixis in *Paspalum notatum*. *BMC Genom.* 20, 487. <https://doi.org/10.1186/s12864-019-5881-0>.
25. Podio, M., Colono, C., Siena, L., Ortiz, J.P.A., and Pessino, S.C. (2021). A study of the heterochronic sense/antisense RNA representation in florets of sexual and apomictic *Paspalum notatum*. *BMC Genom.* 22, 185. <https://doi.org/10.1186/s12864-021-07450-3>.
26. Wójcik, A.N., Nodine, M.D., and Gaj, M.D. (2017). miR160 and miR166/165 contribute to the LEC2-mediated auxin response involved in the somatic embryogenesis induction in *Arabidopsis*. *Front. Plant Sci.* 8, 2024. <https://doi.org/10.3389/fpls.2017.02024>.
27. Wójcikowska, B., and Gaj, M.D. (2017). Expression profiling of AUXIN RESPONSE FACTOR genes during somatic embryogenesis induction in *Arabidopsis*. *Plant Cell Rep.* 36, 843–858. <https://doi.org/10.1007/s00299-017-2114-3>.
28. Damodharan, S., Corem, S., Gupta, S.K., and Arazi, T. (2018). Tuning of SIARF10A dosage by sly-miR160a is critical for auxin-mediated compound leaf and flower development. *Plant J.* 96, 855–868. <https://doi.org/10.1111/tpj.14073>.
29. Mei, S., Zhang, M., Ye, J., Du, J., Jiang, Y., and Hu, Y. (2023). Auxin contributes to jasmonate-mediated regulation of abscisic acid signaling during seed germination in *Arabidopsis*. *Plant Cell* 35, 1110–1133. <https://doi.org/10.1093/plcell/koac362>.
30. Hernandez-Lagana, E., Mosca, G., Mendocilla-Sato, E., Pires, N., Frey, A., Giraldo-Fonseca, A., Michaud, C., Grossniklaus, U., Hamant, O., Godin, C., et al. (2021). Organ geometry channels reproductive cell fate in the *Arabidopsis* ovule primordium. *Elife* 10, e66031. <https://doi.org/10.7554/eLife.66031>.
31. Tucker, M.R., Okada, T., Hu, Y., Scholefield, A., Taylor, J.M., and Koltunow, A.M.G. (2012). Somatic small RNA pathways promote the mitotic events of megagametogenesis during female reproductive development in *Arabidopsis*. *Development* 139, 1399–1404. <https://doi.org/10.1242/dev.075390>.
32. Yang, C., Hu, B., Portheine, S.M., Chuenban, P., and Schnittger, A. (2020). State changes of the HORMA protein ASY1 are mediated by an interplay between its closure motif and PCH2. *Nucleic Acids Res.* 48, 11521–11535. <https://doi.org/10.1093/nar/gkaa527>.
33. De Storme, N., Keçeli, B.N., Zamariola, L., Angenon, G., and Geelen, D. (2016). CENH3-GFP: a visual marker for gametophytic and somatic ploidy determination in *Arabidopsis thaliana*. *BMC Plant Biol.* 16, 1. <https://doi.org/10.1186/s12870-015-0700-5>.
34. Völz, R., Heydlauff, J., Ripper, D., von Lyncker, L., and Groß-Hardt, R. (2013). Ethylene signaling is required for synergid degeneration and the establishment of a pollen tube block. *Dev. Cell* 25, 310–316. <https://doi.org/10.1016/j.devcel.2013.04.001>.
35. Morel, J.B., Godon, C., Mourrain, P., Béclin, C., Boutet, S., Feuerbach, F., Proux, F., and Vaucheret, H. (2002). Fertile hypomorphic ARGONAUTE (*ago1*) mutants impaired in post-transcriptional gene silencing and virus resistance. *Plant Cell* 14, 629–639. <https://doi.org/10.1105/tpc.010358>.
36. Song, J.J., Liu, J., Tolia, N.H., Schneiderman, J., Smith, S.K., Martienssen, R.A., Hannon, G.J., and Joshua-Tor, L. (2003). The crystal structure of the Argonaute2 PAZ domain reveals an RNA binding motif in RNAi effector complexes. *Nat. Struct. Biol.* 10, 1026–1032. <https://doi.org/10.1038/nsb1016>.
37. Pinyopich, A., Ditta, G.S., Savidge, B., Liljegren, S.J., Baumann, E., Wisman, E., and Yanofsky, M.F. (2003). Assessing the redundancy of MADS-box genes during carpel and ovule development. *Nature* 424, 85–88. <https://doi.org/10.1038/nature01741>.
38. Mizzotti, C., Ezquer, I., Paolo, D., Rueda-Romero, P., Guerra, R.F., Battaglia, R., Rogachev, I., Aharoni, A., Kater, M.M., Caporali, E., and Colombo, L. (2014). SEEDSTICK is a master regulator of development and metabolism in the *Arabidopsis* seed coat. *PLoS Genet.* 10, e1004856. <https://doi.org/10.1371/journal.pgen.1004856>.
39. Mendes, M.A., Guerra, R.F., Berns, M.C., Manzo, C., Masiero, S., Finzi, L., Kater, M.M., and Colombo, L. (2013). MADS domain transcription factors mediate short-range DNA looping that is essential for target gene expression in *Arabidopsis*. *Plant Cell* 25, 2560–2572. <https://doi.org/10.1105/tpc.112.108688>.
40. Marconi, G., Capomaccio, S., Comino, C., Acquadro, A., Portis, E., Porceddu, A., and Albertini, E. (2019). Methylation content sensitive enzyme ddRAD (MCSed): a reference-free, whole genome profiling system to address cytosine/adenine methylation changes. *Sci. Rep.* 9, 14864. <https://doi.org/10.1038/s41598-019-51423-2>.
41. Becker, C., Hagmann, J., Müller, J., Koenig, D., Stegle, O., Borgwardt, K., and Weigel, D. (2011). Spontaneous epigenetic variation in the *Arabidopsis thaliana* methylome. *Nature* 480, 245–249. <https://doi.org/10.1038/nature10555>.
42. Schmitz, R.J., Schultz, M.D., Lewsey, M.G., O'Malley, R., Ulrich, M.A., Libiger, O., Schork, N.J., and Ecker, J.R. (2011). Transgenerational epigenetic instability is a source of novel methylation variants. *Science* 334, 369–373. <https://doi.org/10.1126/science.1212959>.
43. Siena, L.A., Michaud, C., Selles, B., Vega, J.M., Pessino, S.C., Ingouff, M., Ortiz, J.P.A., and Leblanc, O. (2023). TRIMETHYLGUANOSINE SYNTHASE1 mutations decanalize female germline development in *Arabidopsis*. *New Phytol.* 240, 597–612. <https://doi.org/10.1111/nph.19179>.
44. Tovar-Aguilar, A., Grimanelli, D., Acosta-García, G., Vielle-Calzada, J.-P., Badillo-Corona, J.A., and Durán-Figueroa, N. (2024). The miRNA822 loaded by ARGONAUTE9 modulates the monosporic female gametogenesis in *Arabidopsis thaliana*. *Plant Reprod.* 37, 243–258. <https://doi.org/10.1007/s00497-023-00487-2>.
45. Su, Z., Wang, N., Hou, Z., Li, B., Li, D., Liu, Y., Cai, H., Qin, Y., and Chen, X. (2020). Regulation of female germline specification via small RNA mobility in *Arabidopsis*. *Plant Cell* 32, 2842–2854. <https://doi.org/10.1105/tpc.20.00126>.
46. Braselton, J.P., Wilkinson, M.J., and Clulow, S.A. (1996). Feulgen staining of intact plant tissues for confocal microscopy. *Biotech. Histochem.* 71, 84–87. <https://doi.org/10.3109/10520299609117139>.
47. Musielak, T.J., Slane, D., Liebig, C., and Bayer, M. (2016). Versatile optical clearing protocol for deep tissue imaging of fluorescent proteins in *Arabidopsis thaliana*. *PLoS One* 11, e0161107. <https://doi.org/10.1371/journal.pone.0161107>.
48. Akalin, A., Kormaksson, M., Li, S., Garrett-Bakelman, F.E., Figueroa, M.E., Melnick, A., and Mason, C.E. (2012). MethylKit: a comprehensive R package for the analysis of genome-wide DNA methylation profiles. *Genome Biol.* 13, R87. <https://doi.org/10.1186/gb-2012-13-10-r87>.
49. Hashimoto, K., Kokubun, S., Itoi, E., and Roach, H.I. (2007). Improved quantification of DNA methylation using methylation-sensitive restriction enzymes and real-time PCR. *Epigenetics* 2, 86–91. <https://doi.org/10.4161/epi.2.2.4203>.

50. Varkonyi-Gasic, E., Wu, R., Wood, M., Walton, E.F., and Hellens, R.P. (2007). Protocol: a highly sensitive RT-PCR method for detection and quantification of microRNAs. *Plant Methods* 3, 12. <https://doi.org/10.1186/1746-4811-3-12>.
51. Galbiati, F., Sinha Roy, D., Simonini, S., Cucinotta, M., Ceccato, L., Cuesta, C., Simaskova, M., Benkova, E., Kamiuchi, Y., Aida, M., et al. (2013). An integrative model of the control of ovule primordia formation. *Plant J.* 76, 446–455.
52. Ezquer, I., Mizzotti, C., Nguema-On, E., Gotté, M., Beuzamy, L., Ebeling Viana, V., Dubrulle, N., Costa de Oliveira, A., Caporali, E., Koroney, A.-S., et al. (2016). The developmental regulator SEEDSTICK controls structural and mechanical properties of the *Arabidopsis* seed coat. *Plant Cell* 28, 2478–2492. <https://doi.org/10.1105/tpc.16.00454>.
53. Newcombe, R.G. (1998). Two-Sided Confidence Intervals for the Single Proportion: Comparison of Seven Methods. *Stat. Med.* 17, 857–872. [https://doi.org/10.1002/\(sici\)1097-0258\(19980430\)17:8<857::aid-sim777>3.0.co;2-e](https://doi.org/10.1002/(sici)1097-0258(19980430)17:8<857::aid-sim777>3.0.co;2-e).

STAR★METHODS

KEY RESOURCES TABLE

REAGENT or RESOURCE	SOURCE	IDENTIFIER
Antibodies		
anti-GFP polyclonal antibody	ChromoTek	RRID: AB_2749857
Chemicals, peptides, and recombinant proteins		
GoTaq DNA Polymerase	Promega	Cat #M3001
Schiff reagent	Merck	1090330500
Renaissance 2200 staining	Renaissance Chemicals	https://www.renchem.co.uk/products/renaissance-SR-2200
miRCURY LNA miRNA Detection Probes	Qiagen	Cat # 339111 YD00612441-BCD
Critical commercial assays		
SV Total RNA Isolation Kit	Promega	Cat #Z3101
Superscript II Reverse transcriptase	Invitrogen	Cat # 18064022
Real Mix qPCR	Biodynamics	Cat # A6101
iTaq SYBR green master mix	Bio-Rad	Cat#1725121
DIG RNA Labeling Kit (SP6/T7)	Roche	Cat#11175025910
Deposited data		
Methylation raw sequence reads	this study	NCBI Database: PRJNA750614 https://www.ncbi.nlm.nih.gov/bioproject/?term=PRJNA750614
Experimental models: Organisms/strains		
<i>Arabidopsis thaliana</i> ARF10:mARF10-GFP line A	The Nottingham Arabidopsis Stock Centre (NASC)	N16288
<i>Arabidopsis thaliana</i> ARF10:mARF10-GFP line B	The Nottingham Arabidopsis Stock Centre (NASC)	N16289
<i>Arabidopsis thaliana</i> Col-0	The Nottingham Arabidopsis Stock Centre (NASC)	
<i>Arabidopsis thaliana</i> pKNU::nlsYFP	Tucker et al., ³¹	
<i>Arabidopsis thaliana</i> pLC2::nlsYFP	Tucker et al., ³¹	
<i>Arabidopsis thaliana</i> ASY3::RFP	Yang et al., ³²	
<i>Arabidopsis thaliana</i> pWOX2::CENH3_GFP	De Storme et al., ³³	
<i>Arabidopsis thaliana</i> FGR7.0	Völz et al., ³⁴	
<i>Arabidopsis thaliana</i> arf10_2	The Nottingham Arabidopsis Stock Centre (NASC)	N655696
<i>Arabidopsis thaliana</i> arf10_3	The Nottingham Arabidopsis Stock Centre (NASC)	N587560
<i>Arabidopsis thaliana</i> stk-2	Pinyopich et al., ³⁷	
<i>Arabidopsis thaliana</i> ago1-27	Morel et al., ³⁵	
Oligonucleotides		
Oligonucleotides for genotyping and expression analyses	See Table S4	
Oligonucleotides for DNA methylation analysis	See Table S4	
Oligonucleotides for Chromatin immunoprecipitation assay	See Table S4	

(Continued on next page)

Continued

REAGENT or RESOURCE	SOURCE	IDENTIFIER
<i>Software and algorithms</i>		
Axiovision 4.1	Carl Zeiss AG	https://www.micro-shop.zeiss.com/it/ch/
LAS AF 2.2.0. A	Leica Microsystems Srl	https://www.leica-microsystems.com/
R version 3.3.2	R Core Team (2023)	www.r-project.org
Methylation Content Sensitive Enzyme Double-Digest Restriction-Site-Associated DNA (ddRAD) technique (MCSeEd)	Pipeline for methylation analysis from raw reads to DMR identification	https://bitbucket.org/capemaster/mcseed/ src/master/
REST-RG 2009	QIAGEN	http://www.REST.de.com
QuantaSoft™	BioRad	https://www.bio-rad.com/en-it/ SearchResults? Text=quantasoft

EXPERIMENTAL MODEL AND STUDY PARTICIPANT DETAILS

Plant material

For *ARF10* expression analysis, we used an Arabidopsis SALK line (NASC ID N16287) transformed with a *pARF10::ARF10_GFP* construct.²¹ The *ARF10* expression re-patterning in the absence of the miR160 function was studied in two different Arabidopsis NASC stocks (N16288, N16289) transformed with *pARF10::mARF10_GFP* fusion constructions, where *ARF10* was mutated to be insensitive to miRNA160.²¹ These transgenic lines express a miR160-resistant form of *ARF10* (*mARF10*), including four silent mutations in the miRNA target site in a Columbia background. During construction, the *mARF10* gene, including the coding region (2.3 kb) and the 5'upstream region (3 kb), was fused to the green fluorescent protein.²¹ We also used specific cell-type reporter lines *pKNU::nlsYFP*,³¹ *pLC2::nlsYFP*,³¹ *ASY3::RFP*,³² *pWOX2::CENH3_GFP*³³ and *FGR7.0*.³⁴ Two defective *arf10* mutant lines (NASC IDs N655696 - *arf10_2* and N587560 - *arf10_3*) were employed to analyze *ARF10* downregulation. The *stk-2*³⁷ and *ago1-27*³⁵ mutants were used in crosses with the *pARF10::ARF10_GFP* line to carry on mechanistic studies. Plants were cultured on soil in growth chambers under a long-day photoperiod (16 h light 22°C/8 h dark 18°C) at 90 μmol photons m⁻² s⁻¹ light intensity using a mix of Sylvania 215-W cool white, fluorescent tubes and 60-W mate bulbs, at the University of Milan facilities.

METHOD DETAILS

Genotyping of *arf10* defective mutants

Genomic DNA was extracted with Edwards Solution [200 mM Tris-HCl (pH 7.5), 250 mM NaCl, 25 mM EDTA, and 0.5% SDS] from one leaf of each plant, precipitated in isopropanol, resuspended, and used in genotyping experiments. Primers flanking both sides of the T insertion for *arf10_2* and *arf10_3* were designed at the T-DNA Primer design page of the Salk Institute Genomic Analysis Laboratory (<http://signal.salk.edu/tdnprimers.2.html>) and are described in Table S4. A primer located inside the T insertion, was used in combination with LP and RP to detect the presence of the insertion. Genomic DNA was amplified with the following primers combinations: 1) LP + LB; 2) RP + LB; 3) LP + RP (Table S4). Plants were classified as homozygous (Hm), heterozygous (Ht), or wild type based on the banding profile.

Microscopy

For DIC microscopy, ovules were clarified with chloral hydrate and examined in a Leica DM2500 microscope equipped with Nomarski differential interference contrast (DIC) optics. For fluorescent microscopy, fresh pistils were collected at different developmental stages for initial fluorescence evaluation, dissected in sterile H₂O + 5% glycerol, and examined in a Nikon fluorescence microscope equipped with Axiovision software. For confocal laser scanning microscopy (CLSM), fresh material was collected, mounted in a 5% glycerol solution, and analysed immediately (to detect the fluorescence signal) or were processed with Feulgen staining (confocal analysis)⁴⁶ to highlight nuclear DNA. The Feulgen technique first dissociate the two strands of DNA through hydrolysis by warm (60°C) 1 M hydrochloric acid, which liberates the hemiacetal functions of deoxyriboses. In an acidic environment, these hemiacetal functions are converted into aldehydic groups through a reversible reaction. Then, the Schiff reagent (i.e., fuchsin decolorated by insertion of a sulfonic group) reacts with the aldehydic groups. According to a possible interpretation, the carbonyl functions interact with the sulfonic groups included in the reagent to form alkyl sulfonic acids, while the chromophore function of the dye is re-established.⁴⁶ Cell walls and meiotic septa were revealed using Renaissance 2200 staining.⁴⁷ CLSM analysis was performed using a Leica TCS SPE microscope with a 488 nm argon laser line for excitation of GFP fluorescence. Emissions were detected between 505 and 580 nm. Images were collected in multi-channel mode, and overlay images were generated using Leica analysis software LAS AF 2.2.0.A.

DNA methylation analysis

Libraries were constructed according to Marconi et al.⁴⁰ The methylation-sensitive enzymes chosen to infer CG, CHG, CHH methylation contexts were *AciI*, *PstI*, and *EcoT22I*, respectively, combined with *MseI* (Table S1). Pooled libraries were purified, size-selected for fragments in the range of 250 bp to 600 bp, quantified, normalized, and amplified with a primer that introduced an Illumina index (at the Y common adapter site) for demultiplexing (Table S4). Samples were then amplified using uniquely indexed primers, pooled, subjected to PCR-enrichment as described by Marconi et al.⁴⁰ and Illumina-sequenced using 150 bp paired-end chemistry. High-quality raw reads from the Illumina sequencing of the CG, CHG, and CHH libraries were analyzed following the protocol and the pipeline described in Marconi et al.⁴⁰ Reads were normalized and filtered, discarding all sites with a co-logarithm of the variation coefficient value higher than -0.35 . The relative methylation levels at each site were calculated following the procedure in Marconi et al.,⁴⁰ and the DMPs (Differentially Methylated Positions; only loci with a False Discovery Rate ≤ 0.05 were considered significant) were called following the MethylKit manual best practices.⁴⁸ The mapping of the DMPs in the same scaffold and closer than a given threshold provided their clustering to identify the DMRs (Differentially Methylated Regions; only loci with a False Discovery Rate ≤ 0.05 were considered significant), based on the procedure reported in Marconi et al.⁴⁰ Statistical analyses were performed in R version 3.3.2 (www.r-project.org) using the 'stats' and 'gplots' packages. The 'stats' package was used to estimate correlations and logistic regression. Complete linkage clustering was carried out using the 'heatmap.2' function of the 'gplots' package, combined with the 'hclust' and 'dist' functions, and with 'ward.D2' as the clustering method. Regarding CHH-DMR validation, as described by Hashimoto et al.,⁴⁹ for each position of the CHH-DMR located 109 bp from the miR160 to be validated, the DNA was digested using *EcoT22I* (the methylation-sensitive enzyme for the corresponding methylcytosine context). The reaction mixture of 25 μ L contained 100 ng DNA, 0.5 U of *EcoT22I* and its relative buffer. For the non-enzyme control (mock), distilled water was added instead of the enzyme. All the samples were then incubated at 37°C for 4 h, follow by heat inactivation at 65°C for 20 min. The Real-time PCR for the methylation status and the relative statistical analysis were performed as in Marconi et al.⁴⁰ The sequence information of the primers that bracketed the enzyme site of each DMP are reported in Table S4. Data are available under the SRA accession number NCBI Database: PRJNA750614.

Silique analysis

The proportion of unfertilized ovules and seeds in the transgenic lines and in homozygous and heterozygous plants was counted with a Leica magnifying stereoscope equipped with a Leica Application Suites software.

qPCR analysis

Oligonucleotides for expression analysis of *ARF10* (AT5G21150) for *arf10_2* and *arf10_3* are described in Table S4. To analyze ARF expression in the N655696 *arf10* homozygous plants, total RNA was extracted from frozen flowers using the SV Total RNA Isolation Kit (PROMEGA) and reverse transcribed with Superscript II (INVITROGEN, Carlsbad, CA, USA) following manufacturer recommendations. Quantitative PCR reactions (final volume: 20 μ L) included 0.5 μ M gene-specific primers, 1X Real Mix qPCR (BIODYNAMICS, Buenos Aires, Argentina) and 20 ng of cDNA. In each experiment, two biological replicates were processed, including three technical replicates and negative control. Amplifications were performed in a Rotor-Gene Q thermocycler (QIAGEN, Hilden, Germany), as follows: 2 min at 94°C followed by 45 cycles of 94°C for 15 s, 57°C for 30 s, and 72°C for 17 s, and a final elongation step of 5 min at 72°C. The specificity of the PCR amplicons was checked by acquiring heat dissociation curves (from 60°C to 95°C). Relative quantitative expression levels were assessed using the REST-RG 2009 software (QIAGEN) with β -*TUBULIN* as an internal reference (Table S4). For the stem-loop PCR we followed the protocol used by Varkonyi-Gasic et al.⁵⁰ and the are available in Table S4.

In situ hybridization

Samples were collected from *ARF10_GFP*, *mARF10_GFP* plants, homozygous *ARF10_GFP stk-2* and homozygous *ARF10_GFP ago1-27* plants. *Arabidopsis thaliana* inflorescences were fixed for 24h in FAA and embedded in paraffin wax as previously described by Galbiati et al.⁵¹ Sections of the embedded material were cut at a thickness of 10 μ m using a microtome and mounted on poly-L-lysine slide (Bio-Optica). Sections were probed with digoxigenin-labeled for *m5GFP* antisense RNA. Hybridization and immunological detection were performed as previously described by Galbiati et al.⁵¹ The *m5GFP* specific antisense probes was amplified respectively with primers mGFP6 FW and RV (Table S4) and transcribed with the DIG RNA Labeling Kit (SP6/T7) by Roche. For the mature miR160 *in situ* hybridization protocol LNA-modified oligonucleotide-based probes were purchased from Qiagen. The slides were observed under a Zeiss Axiophot D1 microscope.

Chromatin immunoprecipitation assay followed by qRT-PCR (ChIP qPCR)

The promoter region of the *ARF10* (2kb upstream to ATG) was analyzed to identify potential CARG boxes. The ChIP experiment was performed as previously described.⁵² One gram of inflorescence till anthesis was used for chromatin extraction from *pSTK::STK-GFP*³⁸ and Col-0 plants. For immunoprecipitation we used 30 μ l of GFP-trap for each sample (ChromoTek). Enrichment of the target regions was calculated by qPCR (iTaQ Universal SYBR Green Supermix, Bio-Rad) using a Bio-Rad iCycler iQ optical system. The relative enrichment of the targets obtained from *pSTK::STK-GFP* inflorescences was compared with the enrichment obtained from WT. *ACTIN 11* was used as reference gene. To establish the efficiency of the chromatin immunoprecipitation, we used the third CARG box of *VDD* as a positive control.¹¹ Three independent ChIP experiments were performed, all the primers used are described in Table S4.

QUANTIFICATION AND STATISTICAL ANALYSIS

Statistical analyses of proportions

Part of the results was analysed using Student's t-test that is performed with Excel (Microsoft), another part using the 95% confidence intervals of the true proportion (95% CI) were calculated according to the Newcombe method⁵³ at the Vassarstats website (<http://vassarstats.net/prop1.html>) and other using one-way ANOVAs with post hoc Turkey test using an online tool (https://astatsa.com/OneWay_Anova_with_TukeyHSD/). Differentially methylated loci significance was calculated using MethylKit R package whereas differentially methylated regions were inferred by logistic regression using R version 3.3.2.